Preclinical Efficacy of IMM-BCP-01, a Highly Active Patient-Derived Anti-SARS-CoV-2 Antibody Cocktail

One sentence summary: We describe three human antibodies that recognize unique non-overlapping epitopes on Spike protein and, when combined, exhibit highly potent *in vitro* activity against multiple SARS-CoV-2 variants of concern, including Delta, that translates into a striking dose-dependent efficacy against two SARS-CoV-2 isolates *in vivo*, augmented by a robust, rare epitope-driven Fc effector response.

Authors: Pavel A. Nikitin[1*], Jillian M. DiMuzio[1], John P. Dowling[1], Nirja B. Patel[1], Jamie L. Bingaman-Steele[1], Baron C. Heimbach[1], Noeleya Henriquez[1], Chris Nicolescu[1], Antonio Polley[1], Raymond J. Howanski[1], Mitchell Nath[1], Halley Shukla[1], James P. Finn[1], Li-fang Liang[1], Todd Smith[1], Nadia Storm[2], Lindsay G. A. McKay[2], Rebecca I. Johnson[2], Lauren E. Malsick[2], Anna N. Honko[2], Anthony Griffiths[2], Purnanand Sarma[1], Dennis H. Geising[1], Michael J. Morin[1], and Matthew K. Robinson[1]

Affiliations:

[1]Immunome, Inc., Exton, PA, U.S.A.

[2]Department of Microbiology, Boston University School of Medicine and National Emerging Infectious Diseases Laboratories, Boston, MA, USA

***Corresponding author**

Email: pnikitin@immunome.com

Abstract

Using an unbiased interrogation of the anti-viral memory B cell repertoire of convalescent COVID-19 patients, we identified three human antibodies that when combined demonstrated both robust viral suppressive properties against all tested SARS-CoV-2 variants of concern *in vitro* and profound anti-viral efficacy *in vivo*. In this report, we describe the pre-clinical characterization of an antibody cocktail, IMM-BCP-01, that consists of three unique, patient-derived recombinant antibodies directed at non-overlapping surfaces on the Spike protein, each with particularly effective antiviral activity. One antibody has a composite epitope blocking ACE2 binding, one antibody bridges two Spike proteins, and one antibody neutralizes virus by binding to a conserved epitope outside of ACE2 binding site. These antibodies, when administered after viral infection, potently decreased viral load in lungs of infected Syrian golden hamsters in a dose-dependent manner, elicited broad anti-viral neutralizing activity against multiple SARS-CoV-2 variants, and induced a robust anti-viral effector function response, including phagocytosis, and activation of classical complement pathway. Our pre-clinical data demonstrate that the unique three antibody cocktail IMM-BCP-01 is a potent and dose-efficient approach to treat early viral infection and prevent SARS-CoV-2 in susceptible individuals.

INTRODUCTION

With over 220 million cases and more than 4.6 million deaths worldwide (Johns Hopkins University Coronavirus Resource Center, Sep 9, 2021), the SARS-CoV-2 viral pandemic continues to pose extraordinary health and economic challenges. The scientific community has risen to face this threat through the discovery and launch of a myriad of vaccines and therapeutics to prevent or treat viral infections. While the early data for the Spike (S) protein-directed vaccines have been impressive, with prophylaxis conferred to 90% or more of recipients, it is expected that 30% or more of people in the US and elsewhere will have "vaccine hesitancy" that will preclude them from seeking vaccination (*1*), while others who are vaccinated will not be fully protected due to a rise of novel vaccine-resistant SARS-CoV-2 variants, immune-insufficiency or other deficits in their response (*2*). Furthermore, recent data suggest that vaccines from some manufacturers may provide weaker protection against new variants of SARS-CoV-2 (*3*, *4*).

As such, the discovery and development of effective antibody therapies for passive immunization is likely to be an important complementary or alternative approach to vaccination. The use of convalescent plasma against SARS-CoV-2 initially yielded mixed results (*5*, *6*), however a recent retrospective cohort study showed reduced mortality in treated patients (*7*) outlining the need for a more robust and more standardized anti-viral antibody cocktail. A monotherapy trial at the US National Institutes of Health with Lilly's Bamlanivimab was halted on the basis of phase 3 data that showed no improvement in clinical outcomes. An early Regeneron trial with a 2-antibody mixture was also paused based on a potential safety signal and an unfavorable risk/benefit profile (Garber, 2021). More recent data have shown, however, that S-protein-directed antibodies can

have significant efficacy and safety, and both the Lilly and Regeneron antibody cocktail candidates received Emergency Use Authorization (EUA) from the US FDA in November 2020, although the EUA for Bamlanivimab has been withdrawn and distribution of the Bamlanivimab/Etesevimab cocktail has been limited to areas where resistant variant frequency is below 5%. Another S-protein specific antibody, sotrovimab, co-developed by Vir and GlaxoSmithKline, received an EUA in May 2021. As publicly reported, Vir is currently developing a second generation antibody aimed to be used in combination with sotrovimab. Finally, the most recent data published by Regeneron demonstrate that both Regeneron 2-Ab cocktail and Vir's VIR-7831 antibody generated escape mutants after seven and two passages *in vitro*, respectively. Hence, Regeneron's publication proposes the addition of the third antibody REGN10985 to the cocktail (*8*). Therefore, the development of a robust three antibody cocktail is the most efficacious anti-viral measure that prevents the generation of viral escape variants.

Even before the widespread use of these prophylactic and therapeutic interventions, with their expected imposition of selection pressure, SARS-CoV-2 was found to undergo steady mutational evolution. In particular, mutations in the S protein have resulted in variant strains that were sometimes more infectious, more virulent or both (*9–13*). The United States Center for Disease Control (CDC) has identified several SARS-CoV-2 variants that they have designated as "Variants of Concern" (VoC), Alpha (B.1.1.7), Beta (B.1.351), Gamma (P.1) and Delta (B.1.617.2) and their sublineages (*14*). As the use of vaccines and antibody monotherapy becomes more widespread, it is expected that additional escape mutants will emerge (Starr et al, 2021; Wang et al, 2021). Such escape mutants are of particular concern if introduced to an unvaccinated population – one that is

expected to persist due to economic or social reasons - and will likely undergo subsequent further changes.

We recently reported the identification of a library of patient-derived anti-viral antibodies (*15*). Based on recent reports (*16*), we hypothesized that deep interrogation of such patient responses would identify rare antibodies against biologically meaningful epitopes that have a synergistic anti-viral effect and are resistant to mutational drift. In this report, we describe the pre-clinical efficacy of three patient-derived antibodies, each selected for its own intrinsic antiviral activity, with intention of developing an antibody cocktail that exhibits robust anti-viral activity *in vitro* and *in vivo* against current isolates and with the potential to treat future variants. These antibodies bind to three non-overlapping epitopes on the receptor binding domain (RBD) and, when combined, potently neutralize all tested viral variants, including all CDC variants of concern (Alpha, Beta, Gamma, Delta and Delta sublineage Delta Plus) and an emerging WHO VOI Lambda *in vitro*, and suppress viral spread in lungs of infected animals when introduced at extremely low doses *in vivo*. Importantly, we observed the drop in viral load in lungs of animals treated with our antibody cocktail in a dose-dependent manner. Mechanistically, each antibody demonstrates unique binding properties: one antibody has a composite epitope involving the ACE2 receptor binding ridge and an area adjacent to the receptor binding loop, one antibody avidly binds to two S proteins within the same spike trimer, and one antibody recognizes a very conserved epitope and induces neutralization without competing for ACE2 binding. Therefore, based on the pre-clinical data, the three antibody cocktail described here is predicted to provide a potent and broad anti-viral therapeutic and prophylactic benefits to patients infected or susceptible to infection with multiple SARS-CoV-2 variants.

RESULTS

IMM-BCP-01 cocktail efficiently suppresses the severity of the disease in an *in vivo* model of SARS-CoV-2.

Using an unbiased interrogation of a previously described library of patient-derived anti-viral antibodies (*15*), we have identified three complementary antibodies, IMM20190, IMM20184 and IMM20253, that had robust combinatorial anti-viral effects. We tested the efficacy of different combinations and doses of these three antibodies in Syrian Golden hamsters infected with SARS-CoV-2 (WA_CDC-WA1/2020) (Figure 1A). When administered to animals 6 hours after viral challenge (treatment paradigm), we observed that a treatment with IMM20190 or 2-Ab combinations comprising IMM20184/IMM20190 and IMM20190/IMM20253 led to robust viral clearance (Figure 1B). However, the most robust clearance was observed with the three Ab cocktail. Five of the six animals in this cohort obtained approximately a 2.5-log reduction of viral titer in the lung on day 4 post viral challenge. In a follow-up study, the 3-Ab cocktail decreased the viral titer in the lungs of animals infected with a high-titer (3.3×10^5 TCID50) of WA_CDC-WA1/2020 by 2-logs. This efficacy was observed when the antibodies were administered at either 1:1:1 ($p=0.0077$) or 1:0.5:0.5 (IMM20190:IMM20184:IMM20253; $p=0.0143$) molar ratios (Figure 1C). However, when subjected to an F-test the variability in clearance level in 1:0.5:0.5 group was higher ($P < 0.0001$) than when the animals were treated with the equimolar ratio cocktail (Figure 1C). When taken together, these data support the IMM-BCP-01 cocktail as comprising all three antibodies at 1:1:1 ratios to obtain the most consistent level of viral clearance.

These studies were carried out using a viral inoculum that was approximately 1-log higher than what is typically used to evaluate efficacy of antibody therapies (*17*, *18*). Therefore, we observed the robust anti-viral effect of our Ab cocktail at higher initial viral loads than reported in other studies. Consistent with the robust activity observed in the context of high viral inoculum, treatment of hamsters with IMM-BCP-01 (0.1 mg each, 0.3 mg total antibody) led to a highly significant ($p<0.0080$) ~3.5 log decrease in viral titer, relative to vehicle-treated controls, in the lungs of animals challenged with levels of virus (3.3×10^4 TCID50 per animal) typically observed in the literature (Figure 1D).

When administered via i.p. injection the IMM-BCP-01 cocktail generally followed first-order absorption and elimination process with a half-life of approximately 100 hours in the hamster model (Supplemental Figure 1). As detailed below, these data suggest that i.p. administration of the 3-Ab cocktail (0.3 mg each) led to serum concentrations in vast excess of the IC50 neutralization concentrations (live virus and pseudovirus) observed for all SARS-CoV-2 variants tested, including the alpha, beta, gamma, and delta variants of concern (Table 1, Figure 2). Surprisingly, across different studies, we observed animals in cohorts treated with IMM-BCP-01 whose lung titers were equivalent to non-treated controls. To better understand that lack of clearance, terminal bleeds were assessed for levels of human IgG in the plasma. Those studies demonstrated that variability in viral clearance was directly correlated with systemic distribution of IMM-BCP-01 (Supplemental Figure 2). Specifically, animals that exhibited decreases in viral lung titers were associated with terminal plasma levels of IMM-BCP-01 greater than 3-5 µg/mL. In contrast, IMM-BCP-01 was not observed at appreciable levels in the blood of animals that failed to clear virus from the lungs. Efficacious levels of IgG in the blood were achieved with

dose levels as low as 0.1 mg each and the data suggest that doses as low as 0.1 mg of each antibody (0.3 mg total dose) are efficacious in both the prophylactic and treatment settings when the drug was absorbed and systemic exposure was achieved (Suppl. Figure 2).

The antibodies comprising IMM-BCP-01 were isolated from convalescent patients early in the pandemic, before the emergence of novel variants. IMM-BCP-01 was designed with the recognition that variants would emerge and that effective treatments would be needed to address them. Consistent with that goal, IMM-BCP-01 exhibits a dose response against both the reference (WA1/2020) and Beta (B.1.351) isolates (Figure 1E, F). The three antibody cocktail suppressed viral titers of both variants in lungs of hamsters treated with doses as low as 0.1 mg of each antibody (0.3 mg total dose). Interestingly, higher doses of IMM-BCP-01 additionally lowered viral load in hamsters infected with both viral isolates in a dose dependent manner. A 4-log reduction in levels of WA1/2020 were achieved with doses of 0.3 mg each and 0.5 mg equimolar dose (1.5 mg total for a IMM20190/184/253 cocktail) potently suppressed (over 700 fold decrease of median value, $p<0.0001$) viral load in lungs of animals infected with Beta variant. We, therefore, observed a clear dose-dependent response *in vivo*, that is in contrast to the previously reported plateaued response in the hamster model of infection (*18*).

The subsequent studies revealed the broad anti-virus effect (Figures 2 and 3) and provided a mechanistic insight on the observed robust *in vivo* efficacy, due to a potent Fc-effector response and non-complementary binding site of antibodies (Figures 4 and 5).

IMM-BCP-01 has a combinatorial neutralizing effect against clinically relevant variants of SARS-CoV-2 virus.

Pseudovirus represent a rapid method for evaluating neutralization potency against newly emerging variants. *In vitro* characterization of the three antibody cocktail demonstrated that IMM-BCP-01 was capable of neutralizing pseudoviruses corresponding to an array of US Center for Disease Control Variants of Concern (VOC) and Variants of Interest (VOI) in a concentration dependent manner (Figure 2A). Of particular note is the activity displayed against the Delta variant, which currently accounts for over 99% of the cases in the United States (CDC website). Strikingly, the 3-Ab cocktail had a modest *increase* in potency against Delta (B.1.617.2), as well as Lambda (C. 37) and Epsilon (B.1.429) pseudoviruses, compared to REF Spike pseudovirus (Figure 2A and Table 1). Overall, IMM-BCP-01 exhibited potent neutralization across the spectrum of variants tested, with all IC50 values being within approximately 1-log of the reference pseudovirus. In context of current landscape of antibody therapeutics for COVID-19, IMM-BCP-01 outperformed S309 against both the Delta and a reference pseudovirus (D614G) when tested in pseudovirus neutralization assays (Figures 2B & 2C). S309 is the parental clone of VIR-7831, which recently obtained an EUA at a lower dose than any of the other antibodies currently in clinical use for treating COVID-19 (*18*).

When extended to intact virus isolates, we observed equivalent, or better potency of the IMM-BCP-01 cocktail against WA1/2020, BavPat (D614G), Alpha (B.1.1.7), Beta (B.1.351) and Gamma (P.1) variants measured in either a spot reduction (Figure 2D, E) or plaque formation assays as compared to the corresponding pseudovirus neutralization assay (Table 1). Activity against Beta (B.1.351) and Gamma (P.1) represented largest drifts in both *in vitro* neutralization potency relative to REF and behavior of the isolates in different assays (Figure 2, Supplemental Figure 4). The 95% CI for the IC50 values for these two variants ranged from 4.9 – 31 nM

depending upon assay format (Table 2). Importantly, *in vitro* neutralization potency against Beta translated into the robust dose response observed against the virus *in vivo* (Figure 1FD). It should also be noted that pseudovirus provided a good surrogate for all viral isolates tested (Figure 2E, Supplemental Figure 4), consistent with prior studies by some authors of this report (*19*). Therefore, while we have not formally tested IMM-BCP-01 against the Delta live virus isolate, the correlation we observe between IC50s of neutralization in both pseudovirus and live virus assays, as well as the translation to *in vivo* efficacy strongly support IMM-BCP-01 will be fully active against the Delta variant.

To better understand the three Ab cocktail, we carried out a series of experiments focused on determining the combinatorial contributions of the component antibodies to the overall neutralizing activity. Specifically, we tested 2-Ab mixtures of IMM20190 (1x concentration) with either IMM20184 (1x) or IMM20253 (1x), and a 3-Ab combination of IMM20190 (1x) with IMM20184/IMM202053 (0.5x each) in pseudovirus neutralization assays (Supplemental Figure 3 and Figure 2E). Double and triple antibody combinations dose-dependently neutralized pseudovirus variants corresponding to three CDC variants of concern (Supplemental Figure 3A, B). We calculated each antibody contribution to the observed neutralizing effect using SynergyFinder 2.0, a previously reported web tool that analyzes the combinatorial effect of different drugs on a phenotype (*20*). The synergy score reflects the effect of different therapeutics on a given measurement. For example, a score below -10 suggests an antagonistic (competitive) effect; a score between -10 and 10 assumes an additive effect; and a score above 10 suggests a synergistic effect of the combined treatment. We detected a concentration-dependent synergistic potential of combinations (Supplemental Figure 3C). In variants where IMM20190 potently

neutralizes, such as REF and Epsilon (B.1.427), antibody combinations are mainly additive, as IMM20190 neutralization was sufficient and did not require the two other antibodies (hence, the observed synergy score was the lowest). In variants where IMM20190 was not as effective, such as B.1.351 (Beta) and P.1 (Gamma), combinations were also additive. In addition, IMM20184 and IMM20253 antibodies as a double combination had an additive neutralizing effect against these variants (Supplemental Figure 3D). Although not formally evaluated for synergy, the combinatorial contribution of the three antibodies was also observed against live Beta and Gamma virus (Supplemental Table 1). Strikingly, we observed the highest synergistic potential of the three antibody combination IMM20190/184/253 for the Alpha (B.1.1.7) variant, where each of the single antibodies neutralized with comparable IC_{50}'s (Figure 2F). In this variant background, the triple antibody combination outperformed all three of the individual antibodies. Thus, the overall combination was able to neutralize all tested variants and induced synergistic effect in a dose-dependent manner (Figure 2F).

IMM20190/184/253 antibody cocktail induces synergistic effector responses *in vitro.*

A growing body of evidence suggests that intact effector function is required for robust viral clearance in animal models of COVID-19 (*21–23*). The antibodies comprising IMM-BCP-01 retain intact IgG1 Fc domains and bind to the RBD in a non-competitive manner (see below) so we hypothesized that IMM2019/184/253 may generate an oligoclonal response to the spike protein that activates productive Fc-mediated effector functions such as phagocytosis (Figure 3A), classical complement pathway activation (Figure 3B) and antibody-dependent cellular cytotoxicity (ADCC, Figure 3C). We tested this hypothesis *in vitro* using standard assays. Particularly, we measured antibody-induced phagocytosis of Trimer-coated beads using a previously published

method (Ackerman et al., 2011). All three human antibodies induced phagocytosis of Trimer-coated beads in a dose-dependent manner relative to an IgG1 isotype control (Figure 3A). Strikingly, even a low (~15 pM) concentration of IMM20253 antibody was sufficient to potently induce phagocytosis. Consistent with the prior *in vitro* and *in vivo* studies, the three antibody cocktail (IMM20190/184/253) demonstrated a higher phagocytic score, compared to a two antibody cocktail (IMM20184/253) or each individual antibody (Figure 3A). We did not observe phagocytosis of Trimer-coated beads in the presence of an IgG1 isotype control antibody.

We next evaluated activation of the classical complement pathway (CP) by IMM20190/184/253 cocktail. We used an adapted CP activation assay (*25*). In brief, we measured deposition of complement component C4 from serum of normal human donors on anti-Spike antibodies bound to Trimer-coated plates. Standalone IMM20190 and IMM20253 antibodies bound to Trimer-coated plates induced a detectable C4 deposition. Further, while IMM20184 bound to Trimer did not activate complement in this assay, the two antibody cocktail IMM20184/253 induced the robust C4 deposition on antibody-Trimer complexes, that was observed at 10-100 fold lower antibody concentration comparing to IMM20190 alone (Figure 3B). Strikingly, the three antibody cocktail IMM20190/184/253 induced a sharp and the most robust activation of the classical complement C4 deposition at 100-1000 fold lower antibody concentration, comparing to IMM20190 alone. This result was reproduced in multiple experiments and suggests the synergistic activation of the classical complement pathway by the two-antibody and, most noticeably, three-antibody cocktails. We did not observe deposition of classical complement component C4 on the isotype control-treated, Trimer-coated surface. Since all tested antibodies used the same heavy chain IgG1 construct, we hypothesized that C4 deposition on Trimer-Ab immune complex may

depend on the Fc epitope conformation and accessibility as previously demonstrated for other systems (*26*, *27*).

We observed similar results in the antibody-dependent cellular cytotoxicity (ADCC) assay, using the reporter Jurkat NFAT-Luc effector and CHO-S1 target cells. IMM20190, but not the isotype control antibody, measurably activated effector cells in the presence of target cells, added at 2:1 (E:T) ratio. IMM20184 and, to a lesser extent, IMM20253, modestly activated effector cells. While the two-antibody combination IMM20184/20253 showed rather additive effect, the three-antibody combination IMM20184/20190/20253 potently activated effector cells at 5-10 fold lower antibody concentration, comparing to IMM20190 alone.

To mechanistically understand the binding properties of IMM20190/20184/20253, we studied individual antibody affinity to soluble RBD or S1 bearing various point mutations in a steady-state Homogeneous Time Resolved Fluorescence (hTRF) assay (Figure 4A and Table 2), measured binding kinetics using SPR approach (Figure 4B and C) and mapped antibody epitopes (Figure 5).

IMM20190, IMM20184 and IMM20253 bind to soluble RBD and S1 protein recapitulating different SARS-CoV-2 variants

Steady-state binding of the three antibodies across a range of variants was characterized via hTRF (Figure 4A and Table 2). Each of the three antibodies was tested for binding against isolated RBD or S1 protein encompassing over 20 different single and multiple mutations that correspond to both naturally occurring and predicted escape mutations. IMM20184 and IMM20253 retained picomolar EC_{50} binding to all single and multiple point mutations tested, including mutations

present in the CDC VOCs and VOI. Furthermore, IMM20253 exhibited some binding to SARS-CoV-1 Spike. In contrast, IMM20190 appeared more susceptible to mutational drift that has occurred to date. Specifically, IMM20190 binding was reduced, to varying degrees, by K417N and the series of RBD-localized mutations associated with either the K417N/E484K/N501Y or K417T/E484K/N501Y variants. Interestingly, binding of IMM20190 appeared to be partially restored for two different S variants containing D614G even in the presence of K417N (Table 2).

Affinity of antibodies

Antibody binding kinetics were measured using a multi-cycle kinetics (MCK) protocol on a Biacore T200 instrument. All three antibodies bound with high affinity to both the isolated RBD and intact spike trimer. (Figure 4B, C). All three antibodies bound with fast on-rates (k_a > 2.95+E4 1/Ms) to the intact trimer, but exhibited even faster on-rates (k_a) to the isolated RBD. This effect was least pronounced for IMM20190, suggesting that its epitope is the most accessible in the intact Trimer structure. IMM20184 and IMM20253 bind to the RBD 17- and 19-times faster than to the Trimer, respectively. Strikingly, the dissociation of IMM20184 from Trimer (k_d^{Trimer} = 2.3E-04 1/s) was 6-times slower as compared to dissociation from RBD (k_d^{RBD} =1.3E-03 1/s). This difference in dissociation suggests the antibody/Trimer complex is stabilized through an avid binding mechanism between the antibody and two subunits of the Trimer. IMM20253, despite exhibiting the greatest difference (19-times) in on-rates between the RBD and Trimer, has the fastest on-rate for the Trimer of all three antibodies. This suggests the epitope is readily accessible in the context of the native Trimer structure.

IMM20190, IMM20184 and IMM20253 antibodies bind to non-competing conserved epitopes

Epitope binning using ForteBio's Octet epitope binning method demonstrated that each of the three antibodies failed to compete for binding and therefore corresponded to unique bins (Figure 5A). To identify the epitopes of IMM20190, IMM20184 and IMM20253 antibodies, we employed a previously reported shotgun mutagenesis approach (Figure 5B). In brief, we used a validated library of RBD (Wuhan/Washington) proteins expressed on the cell surface each containing one amino acid mutation (*16*). Consistent with the epitope binning (Figure 5A), alanine scanning identified unique, non-overlapping epitopes for the three antibodies (Figure 5B). IMM20190 bound to a composite epitope that included the receptor-binding ridge and an area adjacent to the receptor-binding loop (Figure 5B-D). The epitope mapping studies identified 10 residues in the RBD that interacted with IMM20190. Of those 10 residues, 8 are conserved across all CDC VOCs. Two residues, K417 and N501 are mutated, either singly (K417 in alpha/B.1.1.7) or doubly (K417/N501 in beta/B.1.351 and gamma/P.1) in three of the VOCs. The delta variant (B.1.617.2) is conserved with the WA1/2020 reference strain at all 10 residues. The broad epitope may explain the observed resistance of IMM20190 to the majority of single- and double-point mutations within the RBD region (Table 2).

IMM20184 bound to a highly conserved region in the core RBD (Figure 5A-D). The binding site lays in close proximity to the previously reported epitopes of CR3022 and COVA1-16 antibodies that bind to a cryptic epitope on RBD (Figure 5C and Liu et al., 2020; Yuan et al., 2020). In fact, the IMM20184 epitope includes N370, F374, K378, and S383 residues that are completely conserved among all SARS-CoV-2 VOCs (as of September 2021), including Delta variant, SARS-

CoV-1 and related bat and pangolin beta coronaviruses (Figure 5C and Liu et al., 2020). Two remaining residues, A372 and P384, are conserved among all SARS-CoV-2 VOCs, but are different in SARC-CoV-1.

IMM20253 has the highest intrinsic affinity of all three of the antibodies (Figure 4B, C). Interestingly, alanine scanning identified only two residues critical for its binding. The IMM20253 epitope mapped to two residues, K356 and R466, which are conserved among all VOCs and SARS-CoV-1 (Figure 5C). Of note, the R466 residue was conserved among all related sarbeco or lineage b beta-coronaviruses (Figure 5C and (*17*, *28*, *30*)). These residues are located in two peptide motifs, both of which are conserved across two human SARS- and four bat SARS-related coronaviruses (Figure 5B and (*30*)).

We mapped the binding sites of the three antibodies to the previously reported RBD (chain B, PDB 7A97) and Trimer (PDB 7A97) structures (Figure 5D). Based on the location of the epitopes, IMM20190 and IMM20184 likely interfere with RBD binding to ACE2. Further, the apparent avidity-based binding of IMM20184 (Figure 4B) can likely be explained by the close proximity of two of the IMM20184 epitopes present in the 7A97 crystal structure, one of the proteins in the "Up" and the other in the "Down" conformation of Spike proteins within the Trimer (Figure 5D). While the epitope of IMM20253 appears moderately exposed in the "Down" confirmation of the Trimer, it is readily available in the "Up" confirmation (Figure 5D). In fact, IMM20253 epitope location on the outer surface of the "Up" conformation of Trimer may explain a potent induction of phagocytosis and C4 deposition by IMM20253 antibody (Figures 3 and 5D).

IMM20190, IMM20184 and IMM20253 antibody cocktail inhibits RBD Binding to its cellular receptor ACE2

The location of IMM20184 and IMM20190 epitopes suggests that these two antibodies likely block ACE2 binding. To evaluate the interference of each antibody with ACE2 binding, we performed a biochemical ELISA-based receptor inhibition assay. The affinity of a soluble ACE2 protein to REF (Wuhan/Washington), Alpha or UK (B.1.1.7) and Beta or SA (B.1.351) variant RBD coated to an ELISA plate was evaluated in the presence of various concentrations of antibodies of interest. Consistent with hTRF data (Table 2), and its mapped epitope (Figure 5B-D) IMM20184 potently inhibited ACE2 binding to all three RBD variants (Figure 5E). IMM20190 blocked ACE2 binding to REF and UK RBD proteins, and partially modulated ACE2 binding to the SA RBD. In contrast, IMM20253 was unable to fully block ACE2 interactions with any of the three RBD variants tested (Figure 5E). These data are consistent with the location of the IMM20253 epitope relative to the ACE2 binding site, and when taken in context of pseudovirus neutralization as a single agent (Supplemental Figure 3), suggest its neutralization occurs through a distinct mechanism of action. Finally, an equimolar mixture of IMM20190, IMM20185 and IMM20253 antibodies robustly inhibited ACE2 binding to all three tested RBD variants. Importantly, the inhibitory effect of a three antibody cocktail was more pronounced than the effect of each individual antibody that outlines the need for each antibody presence in the final cocktail (Figure 5E). Of note, we detected a minor ACE2 binding preference to B.1.1.7 RBD, comparing to B.1.351 RBD variant (Figure 5E, left panel).

In summary, we have identified three unique antibodies with different mechanisms of action that bind to non-competing epitopes on Spike protein and induce a potent antiviral response *in vitro* and *in vivo*. When combined, the IMM20190/IMM20184/IMM20253 cocktail consistently

showed a robust anti-viral potency *in vivo*, neutralized all VOC (including Delta B.1.617.2 and Delta Plus B.1.617.2.1) tested in pseudovirus and live virus neutralization assays and induced a potent Fc-mediated response, including activation of phagocytosis, and induction of the classical complement pathway.

DISCUSSION

In his "Lessons from the H1N1 Influenza of 2009" published in in 2014, Dr. Harvey Fineberg wrote that "the world was very fortunate that the 2009 H1N1 influenza pandemic was not more severe". Further, he wrote, "[b]y heeding the lessons from the 2009 H1N1 pandemic, the international community will be able to cope more successfully the next time" (*31*). The world, however, was less fortunate during the 2019-2021 pandemic of another RNA virus, SARS-CoV-2, that revealed fractured and, in some instances, misdirected responses to this major disease outbreak. Similar to the influenza virus pandemic, the SARS-CoV-2 outbreak revealed the need for the rapid introduction of therapeutic antibodies to specifically target conserved regions of the virus, be resistant to viral immune escape and inhibit its spread in individuals at risk, such as health care personnel, first responders and immunocompromised individuals (*32*, *33*). Specifically, recent reports outline the need of therapeutic antibody cocktails, as the most reliable and sustainable treatment option (*8*, *16*)

We identified several hundred of anti-SARS-CoV-2 antibodies with diverse anti-viral properties (*15*). Subsequent screening and functional analysis guided us to the selection of three unique, non-competitive anti-Spike antibodies with potent yet complementary anti-viral effects that bound to three spatially distinct surfaces of RBD region of Spike protein (Figure 5D). While each antibody

was capable of neutralizing many variants, including REF, Alpha, Delta, Epsilon and Lambda (Supplemental Figure 3A), the three antibody cocktail IMM20190/184/253 robustly neutralized all variants tested, including all five CDC VOC and two WHO VOI (Figure 2 A-D). Importantly, the range of neutralization potency exhibited by IMM-BCP-01, across the breadth of pseudovirus and live virus tested, translated into robust *in vivo* efficacy in animal models. This was illustrated most notably in the setting of Beta variant. Despite showing a variable level of *in vitro* neutralization potency (4.9 – 24 nM) against the isolate depending on the assay used to measure activity, IMM-BCP-01 exhibited robust *in vivo* efficacy against the live virus at doses consistent with those currently being used in the clinic for other SARS-CoV-2 antibodies.

Each of the three antibodies comprising IMM-BCP-01 appear to elicit viral neutralization through different mechanisms. IMM20190 and IMM20184 antibodies compete with a cellular receptor hACE2 for binding to Spike protein (Figure 5). IMM20190 epitope, identified using a shotgun mutagenesis approach, extends to two surfaces, including the receptor binding ridge of RBD and the region around the receptor-binding loop (*34*). Considering the breadth of this epitope, IMM20190 is expected to be resistant to small changes in the RBD sequence – the result we indeed observed in the biochemical binding experiment (Table 2). The epitope of IMM20184 antibody is located in N370 – P384 region of the RBD, surrounding the RBD core (Figure 5B) that is conserved in all five VOCs of SARS-CoV-2, including Delta (B.1.617.2) variant, and other SARS-related coronaviruses (*28*, *29*). Interestingly, IMM20184 antibody has a higher affinity to a soluble RBD, yet 5.7-fold slower dissociation from a soluble Trimer (Figure 4B), pointing to avid binding to Trimer. In fact, COVA-1 antibody that bound to the area adjacent to IMM20184 epitope has been demonstrated to have a strong cross-neutralizing properties due to avid binding (*28*). The remaining antibody IMM20253 does not directly compete with hACE2 (Figure 5E), but binds to

a conserved epitope (K356 and R466 residues) that is not a common target of the human immune system for generating neutralizing antibodies (*34*). IMM20253 epitope is present in all human as well as in four bat SARS-related coronaviruses (SL-RaTG13, SL-CoVZC45, SL-CoVZXC21 and SL-LYRa3 (Figure 5B,C) (*30*) and is, therefore, expected to be retained in emerging human SARS-related viruses. K356 has been previously shown to participate in a formation of a hydrophobic pocket in the RBD (*35*) that may explain its functional importance and evolutionary conservation. Strikingly, R466 is conserved in all SARS-related pangolin and bat betacoronaviruses, making it an ideal target for the therapeutic intervention. The conserved patch of amino acids around R466 has only rarely elicited an antibody response (*34*). While both residues appear to be moderately available in the "Up" confirmation of Trimer (Figure 5D) the activity associated with IMM20253 points to the availability of its epitope to antibody-based targeting both *in vitro* and *in vivo*. There are two reported antibodies (a nanobody derived from llama and a mouse-derived antibody) that appear to have somewhat overlapping epitopes with IMM20253 (*36*, *37*). However, both described antibodies bound to broader epitopes, i.e more sensitive to mutational drift; both were generated via animal immunizations and need to be tested for off-target binding to human tissues; and either need to be humanized (mouse-derived) or re-designed (llama-derived) prior to being considered for use as therapeutics.

Interestingly, no apparent clinical benefit has been derived by increasing the dose of REGN-CoV2 from 2400 mg to 8000 mg (*38*). Similarly, viral clearance of WA1/2020 elicited by VIR-7831 in hamster studies plateaued at approximately 1.5 log clearance upon treatment with 5 mg/Kg of antibody; increasing to 15 mg/kg led to no better clearance (*18*). In contrast to those findings, administration of IMM-BCP-01, within the 3 – 9 mg/Kg dose range tested, yielded a dose response

of 2.5 – 4 log of clearance of the WA1/2020 virus, with 4-log being at the limit of detection for evaluating absolute clearance levels. Importantly, the dose response was not limited to the WA1/2020 isolate, a similar dose-response was also observed in clearance of Beta variant.

The antibodies selected to comprise IMM-BCP-01 are capable of eliciting additive and synergistic neutralization *in vitro*. While IMM-BCP-01 appears to neutralize virus more effectively than S309, we hypothesize that neutralization potency alone does not account for the overall increase in dose response as compared to what is observed for VIR-7831 in the published literature (*18)*. In fact, published data for REGN10933 and REGN10987, the antibodies comprising REGN-CoV2, suggest they are more potent in *in vitro* neutralization assays (*39*), yet do not appear to lead to significantly higher levels of viral clearance in hamster models of COVID-19 (*40*). As detailed in this study, Fc-mediated viral clearance mechanisms are also enhanced in the context of the IMM-BCP-01 cocktail as compared to any of the three individual antibodies alone. A natural immune response to the virus is polyclonal. It is interesting to speculate that the enhanced viral clearance observed *in vivo* may be a direct result of the oligoclonal nature with which the IMM-BCP-01 antibodies are able to bind to the RBD of Spike. The ability to neutralize via multiple mechanisms leading to synergistic neutralization, in conjunction with the Fc-dependent activation of effector functions, may explain the robust potency detected in the *in vivo* experiments.

In summary, we identified and characterized three potent patient-derived antibodies IMM20190, IMM20184 and IMM20253 with a unique set of anti-viral properties. When combined into the IMM-BCP-01 cocktail, they synergize to neutralize multiple VOCs of SARS-CoV-2, potently activate Fc-mediated anti-viral effector response, and demonstrate impressive anti-viral effect *in vivo*. Based upon the data we have presented, IMM-BCP-01 is efficacious across the spectrum of

variants known to date and based upon the conserved nature of the epitopes it is predicted to be efficacious against future variants. Importantly, recent data support the idea that targeting SARS-CoV-2 with three antibodies should make IMM-BCP-01 much less likely to induce viral escape than targeting with any single or two-antibody cocktail (*8*). Immunome's antibody cocktail may be used in both prophylaxis and therapy setting and has a high potential against prospective SARS-CoV-2 variants.

MATERIAL AND METHODS

Cells

Reporter virus particles (RVP's) were purchased from Integral Molecular, ACE2-293T cells (Integral Molecular; Cat #C-HA102) were cultured in DMEM containing 10% FBS, 10mM HEPES, and 0.5 g/mL Puromycin. Vero E6 cells (BEI resources, NIAID, NIH: VERO C1008 (E6), African green monkey kidney, Working Cell Bank NR-596) were maintained in humidified incubators at 37°C and 5% CO_2 in DMEM high glucose with GlutaMAX and sodium pyruvate (Gibco™, cat #10569) and 10% certified US-origin heat-inactivated fetal bovine serum (Gibco™, cat #10082).

Animal studies

All animal studies described in the manuscript were carried out under Institutional Animal Care and Use Committee (IACUC)-approved protocols at the respective institutions (BU and MRIGlobal) and where appropriate were reviewed and approved by Animal Care and Use Review Office of USAMRDC (ACURO).

Syrian hamster model of SARS-CoV-2 infection

Syrian Golden Hamsters (Envigo) were challenged on Study Day 0 with SARS-CoV-2 via intranasal inoculation, using 0.1 mL in each nare with either 1.67×10^5 or 1.67×10^6 $TCID_{50}$/mL material. Hamsters were treated 6 ± 1 hour after challenge via an intraperitoneal (i.p.) injection. Animals were euthanized on Study Day 4. The lungs were harvested and homogenized for viral titer determination via $TCID_{50}$ assay. Viral clearance levels obtained by the various treatments were compared to non-treated controls using a two-way ANOVA with Tukey's multiple comparisons test. F-tests were performed using an online calculator (https://www.statskingdom.com/220VarF2.html).

Pseudovirus Production and Neutralization Assay

Neutralization experiments using SARS-CoV-2 luciferase reporter virus particles (RVP's) (Integral Molecular) were based on the manufacturer's instructions. In brief, RVP's were thawed for 2-3 minutes in a 37□C water bath. The recommended amount of RVP's was added to the inner wells of a white opaque 96 well plate (Corning; Cat #3917) or 384 well plate (Greiner Bio-One; Cat #781080). Media containing the indicated amount of antibody was added to each well, resulting in a final volume of 100 □L per well (96 well plate) or 25 □L per well (384 well plate). The antibody/RVP mixture was pre-incubated for 1 hour in a 37□C incubator containing 5% CO_2. ACE2-293T target cells were added to each well (2×10^4 cells in 100 □L for a 96 well plate or 0.9×10^4 cells for a 384 well plate) and incubated for 72 hours. Media was removed from all wells, equal volumes of PBS and Renilla-Glo Luciferase Assay Reagent (Promega; Cat #E2720) were added to each well (60 □L total for a 96 well plate or 30 □L total for a 384 well plate). After 10

minutes, luminescence was measured on the EnSpire Plate Reader (PerkinElmer). Percent neutralization was calculated with the following equation: [(RLU of Virus + cells) – (RLU of Experimental Sample)] / [(RLU of Virus + cells) – (RLU of cells only)].

Epitope Mapping of IMM20190, IMM20184 and IMM20253 antibodies

Shotgun Mutagenesis epitope mapping services were provided by Integral Molecular (Philadelphia, PA) as described in (*41*). Briefly, a mutation library of the target protein was created by high-throughput, site-directed mutagenesis. Each residue was individually mutated to alanine, with alanine codons mutated to serine. The mutant library was arrayed in 384-well microplates and transiently transfected into HEK293T cells. Following transfection, cells were incubated with the indicated antibodies at concentrations pre-determined using an independent immunofluorescence titration curve on wild type protein. MAbs were detected using an Alexa Fluor 488-conjugated secondary antibody and mean cellular fluorescence was determined using Intellicyt iQue flow cytometry platform. Mutated residues were identified as being critical to the MAb epitope if they did not support the reactivity of the test MAb but did support the reactivity of the reference MAb. This counter-screen strategy facilitates the exclusion of mutants that are locally misfolded or that have an expression defect.

Calculation of Synergistic Neutralization by Antibody Combinations

In the context of pseudovirus neutralization, synergy between two or three monoclonal antibodies in combination is defined as neutralization that is greater than neutralization by the most effective monoclonal antibody alone. To test whether combinations of antibodies show synergy in neutralizing SARS-CoV-2, we used an approach similar to one described previously (3).

Pseudovirus neutralization experiments were set up as described above, except that multiple monoclonal antibodies were tested in combination. Briefly, for combinations of two antibodies, one test article was titrated in the background of each concentration in a serial dilution of the other test article. Single antibody titrations were included as controls. For combinations of three antibodies, one test article was titrated in the background of each concentration in a serial dilution of a 1:1 mixture of the other two test articles. To evaluate antibody synergy in the combinations, the observed combination response matrix of pseudovirus neutralization was used as input for the online SynergyFinder platform (4), where quadruplicate data points were input separately. The highest single agent (HSA) reference model was applied, which quantifies synergy as the excess over the maximum response of a single drug in the combination. Synergy between antibodies in each combination is reported as an overall synergy score (the average of observed synergy across the dose combination matrix) as well as a peak HSA score (the highest synergy score calculated across the dose combination matrix). Synergy scores of less than -10, between -10 and 10, and greater than 10 indicate antagonistic, additive, and synergistic antibody combinations, respectively. While peak HSA scores report on synergy at the most optimal combination concentrations, the overall synergy score is less affected by outlier data points.

Phagocytosis assay

All Biotinylated antigens tested were diluted to 100 g/mL in PBS + 1% BSA. After overnight incubation on tube rotator in 4 degree Celsius cold room add 1 mL PBS + 1% BSA to each bead-biotinylated antigen mixture. Centrifuge Bead mixtures in a tabletop microcentrifuge at 5000 x g for 20 minutes. Supernatant was discarded. This was repeated for a total of 3 washes, and then bead-antigen mixture was resuspended in 1000 μL of PBS + 1% BSA. Antibodies were diluted to

10 μg/mL in serum free RPMI 1640 and then to 600 ng/mL using the 10 μg/mL working stock. Perform 1:3 dilutions starting with 600 ng/mL. Repeat 6 times for a 7-point curve with a blank being the 8th point on the curve. Add 100 μL of antibody curves to wells on 96well plate. Add 5 μ L of bead-antigen mixture to the appropriate wells for testing. The concentration of beads should be 9.5e5 total per well. The bead-antigen-antibody mixture is incubated at 37C for 2 hours.

15 minutes prior to bead-antibody-antigen mixture being finished, obtain THP-1 Cells and centrifuge cells at 300 x g for 10 minutes. Cells are resuspended at approximately 1e6 cells/mL in serum-free RPMI. Cells are counted on Cellometer 2000 using 20 μl of cells and 20 μL of AOPI using Primary Cell Line settings. THP-1 Cells are then diluted at 2.5e5 cells per mL based on Cellometer count. 100 μL of THP-1 cells at 2.5e5 cells per mL are then added to wells containing bead-antigen-antibody mixture. The bead-antigen-antibody-cells mixture is then incubated at 37□C for 18 hours.

After 18 hours of incubation, plates are centrifuged at 300 x g for 3 minutes. 100 □L of supernatant is removed for possible cytokine analysis. 100 μL of PBS is added and plate is centrifuged at 300 x g for 3 minutes. Supernatant is then aspirated and 200 μL of PBS is added to plate and centrifuged at 300 x g for 3 minutes. Supernatant is aspirated and then 100 μl of Fixation Buffer is added to each well of the plate. Cells are fixed at room temperature for 20 minutes in the dark. After 20 minutes 100 □L of cell staining buffer is added and plate is centrifuged at 300 x g for 3 minutes. Supernatant is aspirated and 200 □L of cell staining buffer is add to each well of the plate and centrifuged at 300 x g for 3 minutes. Supernatant is aspirated and resuspended in 200uL of Cell

Staining buffer. Plate is then run on Attune NXT for acquisition and FCS Files are analyzed using FlowJo Software.

Activation of classical complement pathway

ELISA-based method to evaluate the activation of the classical complement pathway was adapted from (*25*, *42*). Endotoxin-free ELISA plates were coated with wither RBD or Trimer soluble proteins diluted in endotoxin-free PBS (HyClone) overnight. Plates were blocked with endotoxin-free 2% gelatin solution (Sigma) and incubated with anti-Spike antibodies of interest for 1 hour at +4°C. Plates were washed 3 times with endotoxin-free GVB buffer with Ca^{2+} and Mg^{2+} (GVB++, Complement Technology) and incubated with normal human serum (Complement Technology) diluted to 2.5% in GVB++ buffer for 1.5 hours at +37°C on an orbital shaker. Reaction was stopped by a wash with ice-cold PBS. Cells with deposited complement components were stained with anti-C4 antisera (Complement Technology) and a secondary anti-goat-HRP antibody (SouthernBiotech). Plates were incubated with HRP substrate and a stop solution according to manufacturer's instructions (ThermoFisher). Optical density was measured on EnSpire Plate Reader (PerkinElmer).

Evaluation of Antibody-dependent Cellular Cytotoxicity (ADCC)

ADCC was measured using Promega's Reporter bioassay Cat#G7018, V variant according to manufacturer's recommendations. CHO-S1 target cells (Promega Cat #CS3195A06) and Jurkat NFAT-Luc effector cells were mixed at 2:1 (E:T) ratio.

Receptor competition assay

ELISA plates were coated with either REF, UK or SA variant of RBD (SinoBio) overnight and washed with PBS (3x). Single antibody or a 3-Ab cocktail added at equimolar concentrations were added simultaneously with soluble human ACE2 protein (at a concentration of ~ EC80 of its normal binding to RBD protein) and incubated at +37C on an orbital shaker for 1 hour. Plates were washed (3x) and subsequently probed for ACE2 binding with anti-ACE2 antibody.

Authentic virus neutralization assay

Antibody combinations starting at 30 µg/ml per antibody were serially diluted in Dulbecco's Phosphate Buffered Saline (DPBS)(Gibco™) using half-log dilutions. Dilutions were prepared in triplicate for each antibody and plated in triplicate. Each dilution was incubated at 37°C and 5% CO_2 for 1 hour with 1000 plaque forming units/ml (PFU/ml) of each SARS-CoV-2 variant [isolate USA-WA1/2020, hCoV-19/USA/CA_CDC_5574/2020, BEI #NR-54011 "UK" (B.1.1.7) and hCoV-19/South Africa/KRISP-K005325/2020, BEI #NR-54009 "SA" (B.1.351)]. Each virus stock was passaged once from starting material in Vero E6 cells prior to use. Controls included Dulbecco's Modified Eagle Medium (DMEM) (Gibco™) containing 2% fetal bovine serum (Gibco™) and antibiotic-antimycotic (Gibco™) only as a negative control and 1000 PFU/ml SARS-CoV-2 incubated with DPBS. Two hundred microliters of each dilution or control were added to confluent monolayers of NR-596 Vero E6 cells in duplicate and incubated for 1 hour at 37°C and 5% CO_2. The plates were gently rocked every 15 minutes to prevent monolayer drying. The monolayers were then overlaid with a 1:1 solution of 2.5% Avicel® RC-591 microcrystalline cellulose and carboxymethylcellulose sodium (DuPont Nutrition & Biosciences, Wilmington, DE) and 2X Modified Eagle Medium (Temin's modification, Gibco™) supplemented with 2X antibiotic-antimycotic (Gibco™), 2X GlutaMAX (Gibco™) and 10% fetal bovine serum

(Gibco™). Plates were incubated at 37°C and 5% CO2 for 2 days. The monolayers were fixed with 10% neutral buffered formalin and stained with 0.2% aqueous Gentian Violet (RICCA Chemicals, Arlington, TX) in 10% neutral buffered formalin for 30 min, followed by rinsing and plaque counting. The half maximal inhibitory concentrations (IC50) were calculated using GraphPad Prism 8.

REFERENCES AND NOTES

1. T. Callaghan, A. Moghtaderi, J. A. Lueck, P. Hotez, U. Strych, A. Dor, E. F. Fowler, M. Motta, Correlates and disparities of intention to vaccinate against COVID-19. *Soc. Sci. Med.* **272**, 113638 (2021).
2. N. S. Crowcroft, N. P. Klein, A framework for research on vaccine effectiveness. *Vaccine*. **36**, 7286–7293 (2018).
3. J. L. Bernal, N. Andrews, C. Gower, E. Gallagher, R. Simmons, S. Thelwall, J. Stowe, E. Tessier, N. Groves, G. Dabrera, R. Myers, C. N. J. Campbell, G. Amirthalingam, M. Edmunds, M. Zambon, K. E. Brown, S. Hopkins, M. Chand, M. Ramsay, Effectiveness of Covid-19 Vaccines against the B.1.617.2 (Delta) Variant. *https://doi.org/10.1056/NEJMoa2108891*. **385**, 585–594 (2021).
4. R. Rubin, COVID-19 Vaccines vs Variants—Determining How Much Immunity Is Enough. *JAMA*. **325**, 1241–1243 (2021).
5. M. J. Joyner, R. E. Carter, J. W. Senefeld, S. A. Klassen, J. R. Mills, P. W. Johnson, E. S. Theel, C. C. Wiggins, K. A. Bruno, A. M. Klompas, E. R. Lesser, K. L. Kunze, M. A. Sexton, J. C. Diaz Soto, S. E. Baker, J. R. A. Shepherd, N. van Helmond, N. C. Verdun, P. Marks, C. M.

van Buskirk, J. L. Winters, J. R. Stubbs, R. F. Rea, D. O. Hodge, V. Herasevich, E. R. Whelan, A. J. Clayburn, K. F. Larson, J. G. Ripoll, K. J. Andersen, M. R. Buras, M. N. P. Vogt, J. J. Dennis, R. J. Regimbal, P. R. Bauer, J. E. Blair, N. S. Paneth, D. Fairweather, R. S. Wright, A. Casadevall, Convalescent Plasma Antibody Levels and the Risk of Death from Covid-19. *N. Engl. J. Med.* **384**, 1015–1027 (2021).

6. L. M. Katz, (A Little) Clarity on Convalescent Plasma for Covid-19. *N. Engl. J. Med.* **384**, 666–668 (2021).

7. M. A. Thompson, J. P. Henderson, P. K. Shah, S. M. Rubinstein, M. J. Joyner, T. K. Choueiri, D. B. Flora, E. A. Griffiths, A. P. Gulati, C. Hwang, V. S. Koshkin, E. B. Papadopoulos, E. V Robilotti, C. T. Su, E. M. Wulff-Burchfield, Z. Xie, P. P. Yu, S. Mishra, J. W. Senefeld, D. P. Shah, J. L. Warner, COVID-19 and Cancer Consortium, Association of Convalescent Plasma Therapy With Survival in Patients With Hematologic Cancers and COVID-19. *JAMA Oncol.* (2021), doi:10.1001/jamaoncol.2021.1799.

8. R. Copin, A. Baum, A. J. Murphy, G. D. Yancopoulos, C. A. Kyratsous Correspondence, The monoclonal antibody combination REGEN-COV protects against SARS-CoV-2 mutational escape in preclinical and human studies In brief Treatment with monoclonal antibody combinations limits generation of SARS-CoV-2 escape variants in humans and model anima. *Cell*. **184**, 3949-3961.e11 (2021).

9. Q. Li, J. Wu, J. Nie, L. Zhang, H. Hao, S. Liu, C. Zhao, Q. Zhang, H. Liu, L. Nie, H. Qin, M. Wang, Q. Lu, X. Li, Q. Sun, J. Liu, L. Zhang, X. Li, W. Huang, Y. Wang, The Impact of Mutations in SARS-CoV-2 Spike on Viral Infectivity and Antigenicity. *Cell*. **182**, 1284-1294.e9 (2020).

10. B. Korber, W. M. Fischer, S. Gnanakaran, H. Yoon, J. Theiler, W. Abfalterer, N. Hengartner, E. E. Giorgi, T. Bhattacharya, B. Foley, K. M. Hastie, M. D. Parker, D. G. Partridge, C. M. Evans, T. M. Freeman, T. I. de Silva, A. Angyal, R. L. Brown, L. Carrilero, L. R. Green, D. C. Groves, K. J. Johnson, A. J. Keeley, B. B. Lindsey, P. J. Parsons, M. Raza, S. Rowland-Jones, N. Smith, R. M. Tucker, D. Wang, M. D. Wyles, C. McDanal, L. G. Perez, H. Tang, A. Moon-Walker, S. P. Whelan, C. C. LaBranche, E. O. Saphire, D. C. Montefiori, Tracking Changes in SARS-CoV-2 Spike: Evidence that D614G Increases Infectivity of the COVID-19 Virus. *Cell*. **182**, 812-827.e19 (2020).

11. D. N. Fisman, A. R. Tuite, *medRxiv*, in press, doi:10.1101/2021.07.05.21260050.

12. N. G. Davies, C. I. Jarvis, W. J. Edmunds, N. P. Jewell, K. Diaz-Ordaz, R. H. Keogh, Increased mortality in community-tested cases of SARS-CoV-2 lineage B.1.1.7. *Nat. 2021 5937858*. **593**, 270–274 (2021).

13. T. H, W. E, G. M, I. A, F. V, G. J, D. D, P. S, S. EJ, M. N, M. K, von G. A, W. S, A. M, I. A, M. T, G. AJ, E. S, V. Z. G, P. W, P. F, S. A, H. D, M. G, H. NY, K. S, D. MA, T. L, M. I, Y. D, M. C, G. D, A. S, L.-A. O, A.-D. A, G. A, W. CK, S. BT, L. J, A. LCJ, K. P. SL, W. S, M. D, L. RJ, B. JN, W. C, de O. T, Detection of a SARS-CoV-2 variant of concern in South Africa. *Nature*. **592**, 438–443 (2021).

14. SARS-CoV-2 Variant Classifications and Definitions, (available at https://www.cdc.gov/coronavirus/2019-ncov/variants/variant-info.html#Concern).

15. J. M. DiMuzio, B. C. Heimbach, R. J. Howanski, J. P. Dowling, N. B. Patel, N. Henriquez, C. Nicolescu, M. Nath, A. Polley, J. L. Bingaman, T. Smith, B. C. Harman, M. K. Robinson, M. J. Morin, P. A. Nikitin, Unbiased interrogation of memory B cells from convalescent

COVID-19 patients reveals a broad antiviral humoral response targeting SARS-CoV-2 antigens beyond the spike protein. *Vaccine X*, 100098 (2021).

16. Z. Ku, X. Xie, E. Davidson, X. Ye, H. Su, V. D. Menachery, Y. Li, Z. Yuan, X. Zhang, A. E. Muruato, A. G. i Escuer, B. Tyrell, K. Doolan, B. J. Doranz, D. Wrapp, P. F. Bates, J. S. McLellan, S. R. Weiss, N. Zhang, P. Y. Shi, Z. An, Molecular determinants and mechanism for antibody cocktail preventing SARS-CoV-2 escape. *Nat. Commun.* **12**, 1–13 (2021).

17. C. Garrett Rappazzo, L. V. Tse, C. I. Kaku, D. Wrapp, M. Sakharkar, D. Huang, L. M. Deveau, T. J. Yockachonis, A. S. Herbert, M. B. Battles, C. M. O'Brien, M. E. Brown, J. C. Geoghegan, J. Belk, L. Peng, L. Yang, Y. Hou, T. D. Scobey, D. R. Burton, D. Nemazee, J. M. Dye, J. E. Voss, B. M. Gunn, J. S. McLellan, R. S. Baric, L. E. Gralinski, L. M. Walker, Broad and potent activity against SARS-like viruses by an engineered human monoclonal antibody. *Science (80-.).* **371**, 823–829 (2021).

18. A. L. Cathcart, C. Havenar-Daughton, F. A. Lempp, D. Ma, M. Schmid, M. L. Agostini, B. Guarino, J. Di iulio, L. Rosen, H. Tucker, J. Dillen, S. Subramanian, B. Sloan, S. Bianchi, J. Wojcechowskyj, J. Zhou, H. Kaiser, A. Chase, M. Montiel-Ruiz, N. Czudnochowski, E. Cameroni, S. Ledoux, C. Colas, L. Soriaga, A. Telenti, S. Hwang, G. Snell, H. W. Virgin, D. Corti, C. M. Hebner, *bioRxiv*, in press, doi:10.1101/2021.03.09.434607.

19. S. Clark, L. Clark, J. Pan, A. Coscia, L. McKay, S. Shankar, R. Johnson, V. Brusic, M. Choudhary, J. Regan, J. Li, A. Griffiths, J. Abraham, SARS-CoV-2 evolution in an immunocompromised host reveals shared neutralization escape mechanisms. *Cell*. **184**, 2605-2617.e18 (2021).

20. A. Ianevski, A. K. Giri, T. Aittokallio, SynergyFinder 2.0: Visual analytics of multi-drug

combination synergies. *Nucleic Acids Res.* **48**, W488–W493 (2021).

21. E. S. Winkler, P. Gilchuk, J. Yu, A. L. Bailey, R. E. Chen, Z. Chong, S. J. Zost, H. Jang, Y. Huang, J. D. Allen, J. B. Case, R. E. Sutton, R. H. Carnahan, T. L. Darling, A. C. M. Boon, M. Mack, R. D. Head, T. M. Ross, J. E. Crowe, M. S. Diamond, Human neutralizing antibodies against SARS-CoV-2 require intact Fc effector functions for optimal therapeutic protection. *Cell*. **184**, 1804-1820.e16 (2021).

22. A. Schäfer, F. Muecksch, J. C. C. Lorenzi, S. R. Leist, M. Cipolla, S. Bournazos, F. Schmidt, A. Gazumyan, R. S. Baric, D. F. Robbiani, T. Hatziioannou, J. V. Ravetch, P. D. Bieniasz, M. C. Nussenzweig, T. P. Sheahan, Antibody potency, effector function and combinations in protection from SARS-CoV-2 infection in vivo. *bioRxiv* (2020), , doi:10.1101/2020.09.15.298067.

23. R. Yamin, A. T. Jones, H.-H. Hoffmann, K. S. Kao, R. L. Francis, T. P. Sheahan, R. S. Baric, C. M. Rice, J. V Ravetch, S. Bournazos, R. J, Y. R, J. A, H. HH, K. K, F. R, S. T, B. R, R. C, B. S, Fc-engineered antibody therapeutics with improved efficacy against COVID-19 (2021), doi:10.21203/RS.3.RS-555612/V1.

24. M. E. Ackerman, B. Moldt, R. T. Wyatt, A. S. Dugast, E. McAndrew, S. Tsoukas, S. Jost, C. T. Berger, G. Sciaranghella, Q. Liu, D. J. Irvine, D. R. Burton, G. Alter, A robust, high-throughput assay to determine the phagocytic activity of clinical antibody samples. *J. Immunol. Methods*. **366**, 8–19 (2011).

25. P. A. Nikitin, E. L. Rose, T. S. Byun, G. C. Parry, S. Panicker, C1s Inhibition by BIVV009 (Sutimlimab) Prevents Complement-Enhanced Activation of Autoimmune Human B Cells In Vitro. *J. Immunol.* **202**, 1200–1209 (2019).

26. G. Wang, R. N. De Jong, T. J. Van Den Bremer, J. Schuurman, P. W. H. I. Parren, A. J. R. Heck, E. T. J. Van Den Bremer, F. J. Beurskens, A. F. Labrijn, D. Ugurlar, P. Gros, Molecular Basis of Assembly and Activation of Complement Component C1 in Complex with Immunoglobulin G1 and Antigen Article Molecular Basis of Assembly and Activation of Complement Component C1 in Complex with Immunoglobulin G1 and Antigen. *Mol. Cell*. **63**, 135–145 (2016).

27. C. A. Diebolder, F. J. Beurskens, R. N. De Jong, R. I. Koning, K. Strumane, M. A. Lindorfer, M. Voorhorst, D. Ugurlar, S. Rosati, A. J. R. Heck, J. G. J. Van De Winkel, I. A. Wilson, A. J. Koster, R. P. Taylor, E. O. Saphire, D. R. Burton, J. Schuurman, P. Gros, P. W. H. I. Parren, Complement is activated by IgG hexamers assembled at the cell surface. *Science (80-.).* **343**, 1260–1263 (2014).

28. H. Liu, N. C. Wu, M. Yuan, S. Bangaru, J. L. Torres, T. G. Caniels, J. van Schooten, X. Zhu, C. C. D. Lee, P. J. M. Brouwer, M. J. van Gils, R. W. Sanders, A. B. Ward, I. A. Wilson, Cross-Neutralization of a SARS-CoV-2 Antibody to a Functionally Conserved Site Is Mediated by Avidity. *Immunity*. **53**, 1272-1280.e5 (2020).

29. M. Yuan, N. C. Wu, X. Zhu, C. C. D. Lee, R. T. Y. So, H. Lv, C. K. P. Mok, I. A. Wilson, A highly conserved cryptic epitope in the receptor binding domains of SARS-CoV-2 and SARS-CoV. *Science (80-.).* **368**, 630–633 (2020).

30. J. A. Jaimes, N. M. André, J. S. Chappie, J. K. Millet, G. R. Whittaker, Phylogenetic Analysis and Structural Modeling of SARS-CoV-2 Spike Protein Reveals an Evolutionary Distinct and Proteolytically Sensitive Activation Loop. *J. Mol. Biol.* **432**, 3309–3325 (2020).

31. H. V. Fineberg, Pandemic Preparedness and Response — Lessons from the H1N1

Influenza of 2009. *N. Engl. J. Med.* **370**, 1335–1342 (2014).

32. M. Marovich, J. R. Mascola, M. S. Cohen, Monoclonal Antibodies for Prevention and Treatment of COVID-19. *JAMA - J. Am. Med. Assoc.* **324** (2020), pp. 131–132.

33. B. Sawitzki, S. Schlickeiser, P. Reinke, H.-D. Volk, Monitoring tolerance and rejection in organ transplant recipients. *Biomarkers* (2011) (available at http://www.tandfonline.com/doi/full/10.3109/1354750X.2011.578754).

34. A. J. Greaney, A. N. Loes, K. H. D. Crawford, T. N. Starr, K. D. Malone, H. Y. Chu, J. D. Bloom, Comprehensive mapping of mutations in the SARS-CoV-2 receptor-binding domain that affect recognition by polyclonal human plasma antibodies (2021), doi:10.1016/j.chom.2021.02.003.

35. J. Zahradník, S. Marciano, M. Shemesh, E. Zoler, J. Chiaravalli, B. Meyer, O. Dym, N. Elad, G. Schreiber, SARS-CoV-2 RBD in vitro evolution follows contagious mutation spread, yet generates an able infection inhibitor. *bioRxiv* (2021), doi:10.1101/2021.01.06.425392.

36. D. Sun, Z. Sang, Y. J. Kim, Y. Xiang, T. Cohen, A. K. Belford, A. Huet, J. F. Conway, J. Sun, D. J. Taylor, D. Schneidman-Duhovny, C. Zhang, W. Huang, Y. Shi, Potent neutralizing nanobodies resist convergent circulating variants of SARS-CoV-2 by targeting diverse and conserved epitopes. *Nat. Commun. 2021 121*. **12**, 1–14 (2021).

37. V. L, A. L, L. Z, C. RE, G. P, R. S, S. B, Z. H, C. JB, W. ES, W. B, D. L, A. I, S. PY, C. A, P. A, H. S, W. D, B. A, C. JE, W. SPJ, F. D, D. M, A potently neutralizing anti-SARS-CoV-2 antibody inhibits variants of concern by binding a highly conserved epitope. *bioRxiv Prepr. Serv. Biol.* (2021), doi:10.1101/2021.04.26.441501.

38. D. M. Weinreich, S. Sivapalasingam, T. Norton, S. Ali, H. Gao, R. Bhore, B. J. Musser, Y.

Soo, D. Rofail, J. Im, C. Perry, C. Pan, R. Hosain, A. Mahmood, J. D. Davis, K. C. Turner, A. T. Hooper, J. D. Hamilton, A. Baum, C. A. Kyratsous, Y. Kim, A. Cook, W. Kampman, A. Kohli, Y. Sachdeva, X. Graber, B. Kowal, T. DiCioccio, N. Stahl, L. Lipsich, N. Braunstein, G. Herman, G. D. Yancopoulos, REGN-COV2, a Neutralizing Antibody Cocktail, in Outpatients with Covid-19. *https://doi.org/10.1056/NEJMoa2035002*. **384**, 238–251 (2020).

39. J. Hansen, A. Baum, K. E. Pascal, V. Russo, S. Giordano, E. Wloga, B. O. Fulton, Y. Yan, K. Koon, K. Patel, K. M. Chung, A. Hermann, E. Ullman, J. Cruz, A. Rafique, T. Huang, J. Fairhurst, C. Libertiny, M. Malbec, W. Lee, R. Welsh, G. Farr, S. Pennington, D. Deshpande, J. Cheng, A. Watty, P. Bouffard, R. Babb, N. Levenkova, C. Chen, B. Zhang, A. R. Hernandez, K. Saotome, Y. Zhou, M. Franklin, S. Sivapalasingam, D. C. Lye, S. Weston, J. Logue, R. Haupt, M. Frieman, G. Chen, W. Olson, A. J. Murphy, N. Stahl, G. D. Yancopoulos, C. A. Kyratsous, Studies in humanized mice and convalescent humans yield a SARS-CoV-2 antibody cocktail. *Science*. **369**, 1010 (2020).

40. A. Baum, D. Ajithdoss, R. Copin, A. Zhou, K. Lanza, N. Negron, M. Ni, Y. Wei, K. Mohammadi, B. Musser, G. S. Atwal, A. Oyejide, Y. Goez-Gazi, J. Dutton, E. Clemmons, H. M. Staples, C. Bartley, B. Klaffke, K. Alfson, M. Gazi, O. Gonzalez, E. Dick, Jr., R. Carrion, Jr., L. Pessaint, M. Porto, A. Cook, R. Brown, V. Ali, J. Greenhouse, T. Taylor, H. Andersen, M. G. Lewis, N. Stahl, A. J. Murphy, G. D. Yancopoulos, C. A. Kyratsous, REGN-COV2 antibodies prevent and treat SARS-CoV-2 infection in rhesus macaques and hamsters. *Science*. **370**, 1110 (2020).

41. E. Davidson, B. J. Doranz, A high-throughput shotgun mutagenesis approach to mapping B-cell antibody epitopes. *Immunology*. **143**, 13–20 (2014).

42. J. Shi, E. L. Rose, A. Singh, S. Hussain, N. E. Stagliano, G. C. Parry, S. Panicker, TNT003, an inhibitor of the serine protease C1s, prevents complement activation induced by cold agglutinins. *Blood*. **123**, 4015–4022 (2014).

ACKNOWLEDMENTS

This study was funded by the U.S. Department of Defense (DOD) Joint Program Executive Office for Chemical, Biological, Radiological and Nuclear Defense's (JPEO-CBRND) Joint Project Manager for Chemical, Biological, Radiological and Nuclear Medical (JPEO-CBRN Medical), in collaboration with the Defense Health Agency (DHA), under contract W911QY2090019. The opinions, interpretations, conclusions and recommendations are those of the authors and are not necessarily endorsed by the U.S. Army.

The following reagents were obtained through BEI Resources, NIAID, NIH: VERO C1008 (E6), Kidney (African green monkey), Working Cell Bank, NR-596; SARS-CoV-2, Isolate hCoV-19/USA/CA_CDC_5574/2020, NR-54011 (deposited by Centers for Disease Control and Prevention) and SARS-CoV-2, Isolate hCoV-19/South Africa/KRISP-K005325/2020, NR-54009 (contributed by Alex Sigal and Tulio de Oliveira). The SARS-CoV-2 isolate USA-WA1/2020 starting material was provided by the World Reference Center for Emerging Viruses and Arboviruses (WRCEVA), with Natalie Thornburg (nax3@cdc.gov) as the CDC Principal Investigator.

AUTHOR CONTRIBUTIONS

PAN, JMD, JPD, NBP, JLBS, BCH, NH, CN, AP, RJH, MN, HS, JPF, TS, NS, LGAM, RIJ and LEM performed wet laboratory experiments. PAN, JMD, JPD, JLBS, AHN, AG and MKR analyzed and interpreted the data. LFL, AG and DHG consulted and critically discussed the manuscript. PAN, JDM, PS, MJM and MKR supervised the project. PAN, JDM, JPD, JLBS and MKR wrote and AG, DHG, PS and MJM edited the manuscript. The manuscript was reviewed and cleared for publication by DoD's JPEO-CBRN Medical, JPEO-CBRND.

COMPETING INTEREST STATEMENT

The described approach, antibodies and cocktail composition have been included in patent applications. PAN, JMD, JPD, NBP, JLBS, BCH, NH, CN, AP, MN, HS, JPF, LFL, TS, PS, DHG, MJM and MKR are employees and shareholders of Immunome, Inc.

TABLES

Table 1. IC50 Values (nM) for IMM-BCP-01 Against Reference and VOC viruses. Shown values are Means and 95% confidence intervals.

	Spike Pseudovirus	SARS-CoV-2 ViroSpot	SARS-CoV-2 Plaque Forming Units
Isolate	IC_{50}	IC_{50}	IC_{50}
REF (WA1/2020)	1 (0.7-1.3)	N/T	1.0 (0.8-1.3)
D614G (BavPat-1)	0.9 (0.7 - 1.1)	0.3 (0.2-0.4)	N/T
Alpha (B.1.1.7)	3.4 (2.4-4.3)	0.4 (0.2-0.7)	3.1 (2.4-4.0)
Beta (B.1.351)	13.5 (7.2-20)	22.2 (19.0-24.0)	7.4 (4.9-11.4)
Gamma (P.1)	24.8 (16-31)	5.3 (< 6.7)	N/T
Delta (B.1.617.2)	0.4 (0.3-0.5)	N/T	N/T
Delta plus (B.1.617.2.1)	3 (2.0-3.9)	N/T	N/T
Epsilon (B.1.429)	0.6 (0.5-0.7)	N/T	N/T
Kappa (L452R/E484Q)	1 (0.6 - 1.3)	N/T	N/T
Lambda (C.37)	0.4 (0.3-0.5)	N/T	N/T

Table 2. Breadth of binding of IMM20190/184/253 antibodies to RBD proteins corresponding to CDC variants of concern. EC50 (pM) relative to respective reference proteins measured using hTRF assay.

Sort	His-tagged protein	Binding region	Variant	IMM20190	IMM20253	IMM20184
1	A352S	RBD		25.4	33.0	27.7
2	A475V	RBD	LY escape-3	70.2	34.6	30.3
3	E406Q	RBD		67.2	44.1	29.2
4	E484K	RBD	South Africa (beta), Brazil (gamma)	39.2	32.7	23.2
5	E484Q	RBD	India (B.1.617)	59.9	22.7	21.0
6	F486S	RBD		41.2	26.3	23.0
7	F490S	RBD	Peru (lambda)	14.7	73.4	60.8
8	K417N	RBD	South Africa (beta), India (delta+)	>500	67.4	44.3
9	K417N, E484K, N501Y	RBD	South Africa (beta)	not detected	25.0	20.7
10	K417T, E484K, N501Y	RBD	Brazil (gamma)	>500	22.6	17.9
11	K444R	RBD		33.9	26.7	20.9
12	L452R	RBD	USA (epsilon), India (all)	40.9	34.3	41.2
13	L452R, T478K	RBD	India (B.1.617.2, delta)	52.8	61.7	111
14	N439K	RBD	Scotland, Europe	76.6	56.5	52.1
15	N440K	RBD		45.6	39.7	32.1
16	N501Y	RBD	UK (alpha), SA (beta), Brazil gamma)	311	59.0	42.2
17	Spike RBD (319-591)	RBD	Wuhan / Washington reference	69.9	53.4	46.2
18	T478I	RBD		16.4	45.5	68.5
19	Y453F	RBD	Denmark (mink)	71.6	65.6	50.1
20	A222S, D614G	S1	Europe, Spain	51.0	45.1	29.9
21	D614G	S1	Multiple	69.9	62.9	44.1
22	K417N, E484K, N501Y, D614G	S1	South Africa (beta)	391	34.7	25.6
23	Spike S1 (WT)	S1	Wuhan / Washington reference	58.8	50.0	34.4
24	SARS-CoV-1	S1	Wild type	not detected	137.0	>500
25	T19R, G142D, E156G, Δ157-158, L452R, T478K, D614G, P681R	S1	India (B.1.617.2, delta)	22.2	40.9	30.6
26	E154K, L452R, E484Q, D614G, P681R	S1	India (B.1.617.1, kappa)	38.2	49.2	22.7
27	ΔHV69/70, Y453F, D614G	S1	Denmark (mink)	48.1	67.1	34.8
28	ΔHV69/70, ΔY144, N501Y, A570D, D614G, P681H	S1	UK (alpha)	>500	63.1	49.1

FIGURES AND FIGURE LEGENDS

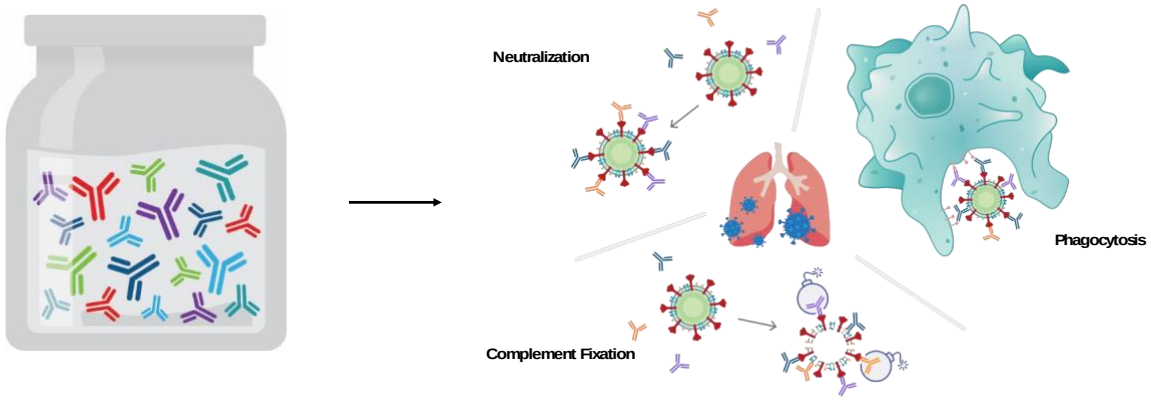

Graphical Abstract

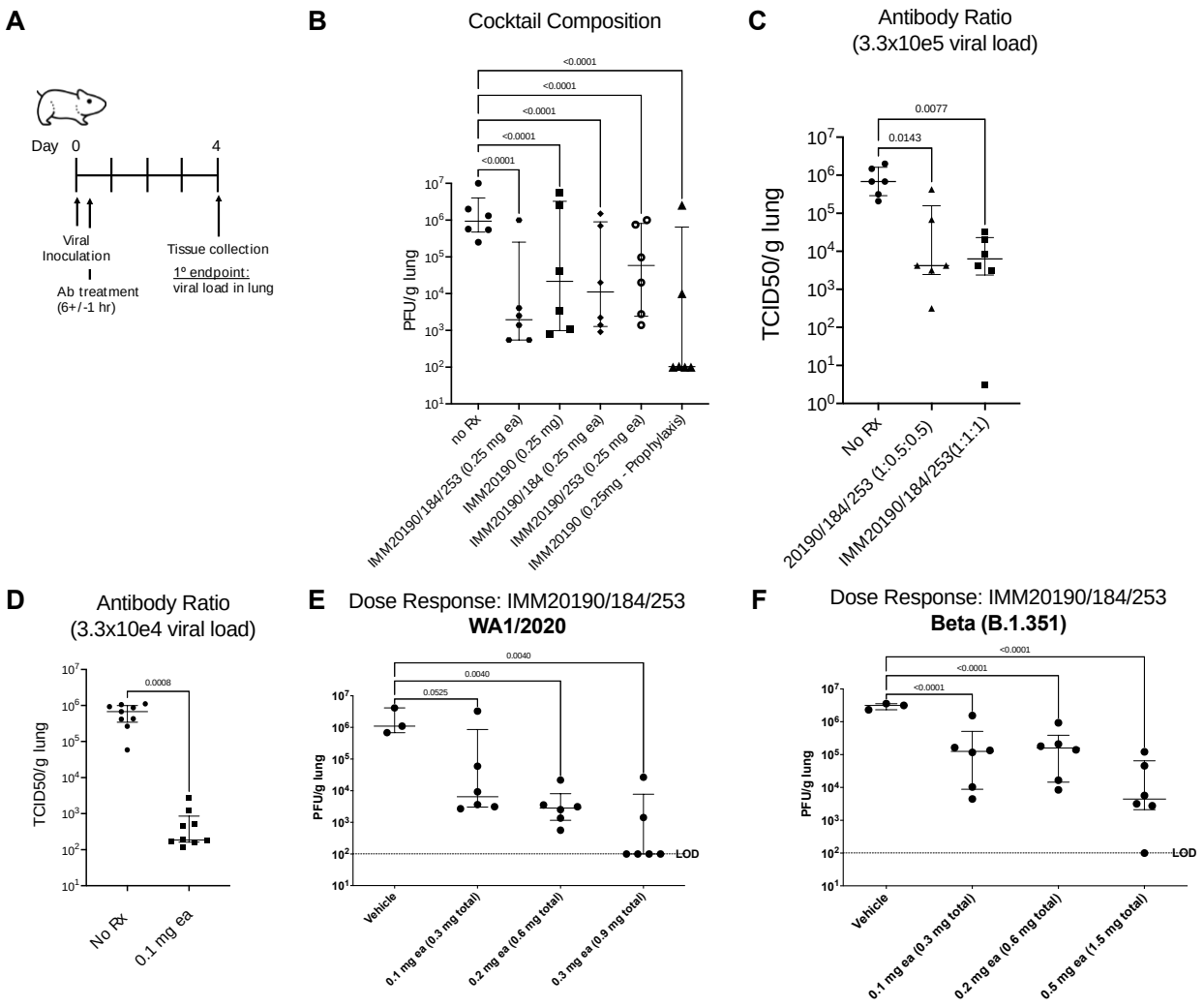

Figure 1. Three antibody combinations IMM20190/184/253 inhibits replication of non-adapted SARS-CoV-2 in lungs of infected animals. (A) All studies were carried out in Syrian Golden hamsters challenged with an intra-nasal inoculation of SARS-CoV-2 and treated with antibodies post-inoculation. Lungs were harvested at Day 4 and viral titers determined by either plaque forming or TCID50 assays. (B) Animals were infected with WA_CDC-WA1/2020 isolate and treated with single, double, or triple antibody cocktails, as noted, 6 hours post-inoculation. (C) Hamsters were challenged with 3.3 x 10^5 TCID50 viral inoculation and treated with 3-Ab cocktail, at two different antibody ratios (1:1:1 or 1:0.5:0.5). (D) Hamsters were challenged with 3.3 x 10^4

TCID50 viral inoculation and treated with 3-Ab cocktail at 1:1:1 ratio, at 0.1 mg dose each (0.3 mg total). (E) and (F) Hamsters were challenged with 10e4 PFU of WA1/2020 (E) or Beta (B.1.351) SARS-CoV-2 isolates and treated with different doses of 3-Ab cocktail IMM20190/184/253 at 1:1:1 ratio. Bar denotes median values. Error bars denote interquartile range. Statistical analysis in panel B is Two-Way ANOVA and in panels C-F is One-way ANOVA using Dunnet's multiple comparisons test comparing to untreated group (No Rx) available in Prizm 9.

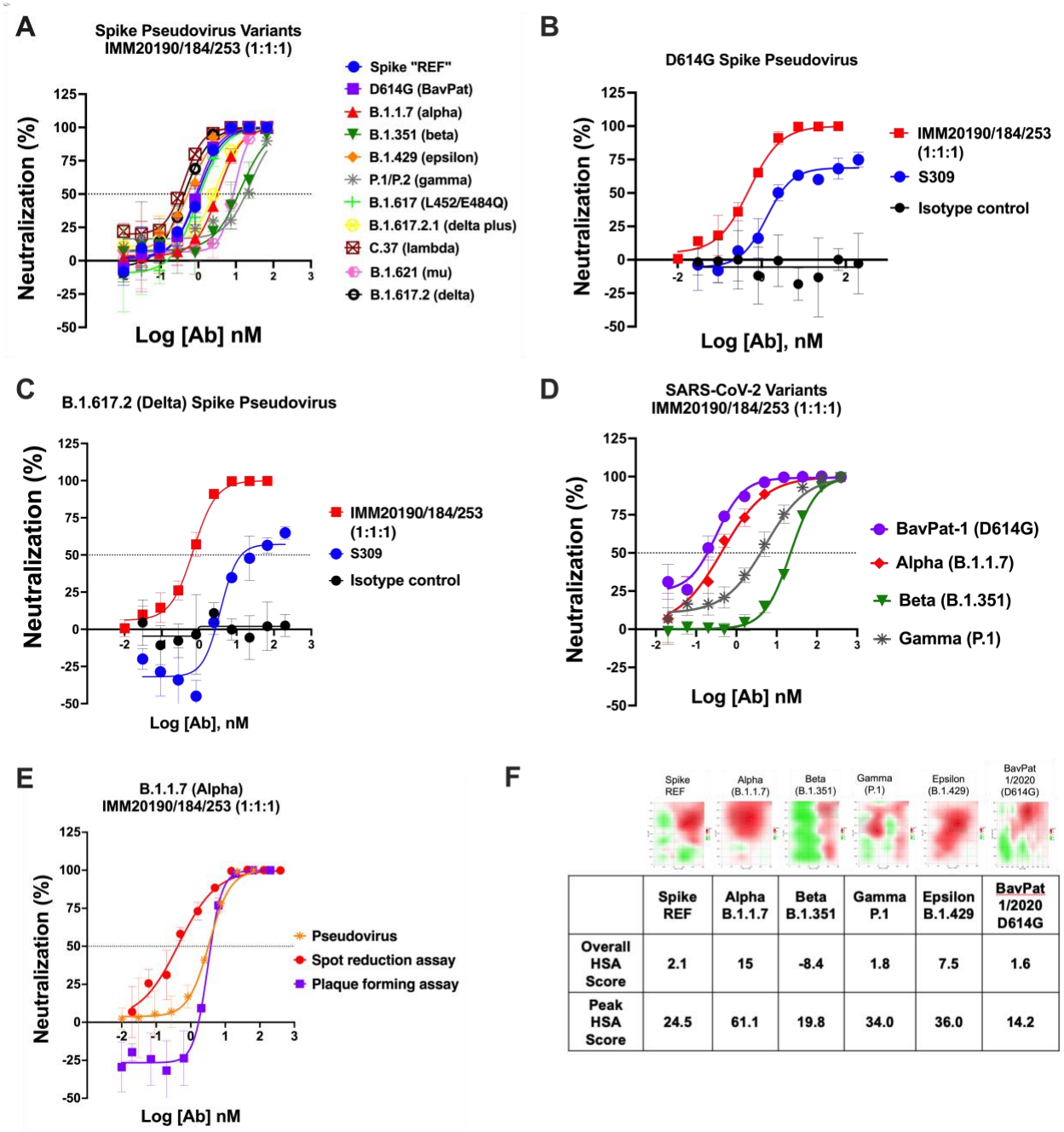

	Spike REF	Alpha B.1.1.7	Beta B.1.351	Gamma P.1	Epsilon B.1.429	BavPat 1/2020 D614G
Overall HSA Score	2.1	15	-8.4	1.8	7.5	1.6
Peak HSA Score	24.5	61.1	19.8	34.0	36.0	14.2

Figure 2. Immunome antibody combination has a synergistic effect against clinically relevant SARS-CoV-2 variants. (A) IMM20190/184/253 neutralization of Spike pseudoviruses that correspond to CDC VOCs and VOI. (B), (C) Neutralization of D614G (B) and Delta Spike (C) pseudovirus by Immunome's three antibody cocktail IMM20190/184 and S309 antibodies. Shown

data are representative experiments of two independent repeats. (D) Neutralization of VOC isolates of SARS-CoV-2 by IMM20190/184/253 cocktail as measured by ViroSpot assay. Antibodies are mixed at equimolar ratio. (E) Neutralization of Alpha (B.1.1.7) variant by IMM20190/184/253 cocktail measured with three different methods, including a pseudovirus neutralization, intact virus spot reduction (ViroSpot) and intact virus plaque formation assays. (F) Synergy scores of the 3-Ab cocktail IMM20190/184/253 against 5 pseudoviruses and one BavPat1/2020 (D614G) live virus isolate calculated with SynergyFinder 2.0 online tool. HSA, the highest single agent model score, calculates the excess over the maximum single antibody response. HSA score below -10 indicates competition; between -10 to 10 shows additive effect; and above 10 demonstrates synergy among tested agents.

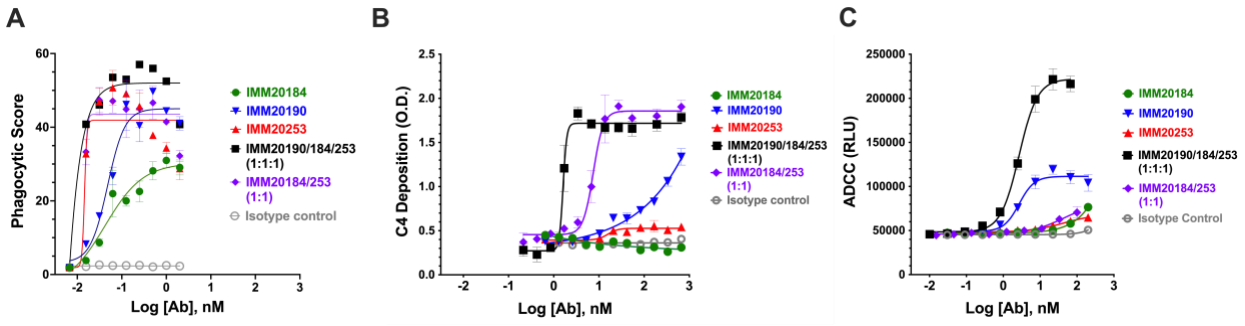

Figure 3. Three antibody cocktail induces synergistic effector function responses *in vitro.* (A) Opsonization with single IMM antibodies, two antibody- (IMM20184/20253) and three-antibody (IMM190/184/253) combinations induce phagocytosis of Trimer-coated beads. (B) Deposition of classical complement component C4 on IMM antibodies bound to Trimer-coated surface. Denoted points represent Mean values; error bars are SEM. **(C)** IMM antibody- or antibody combination-dependent cellular cytotoxicity (ADCC), measured using Jurkat NFAT-Luc reporter effector cells

and Spike-expressing target cells at 2:1 (E:T) ratio. Molarity shown is molarity of each cocktail. Denoted points represent Mean values; error bars are St.Dev.

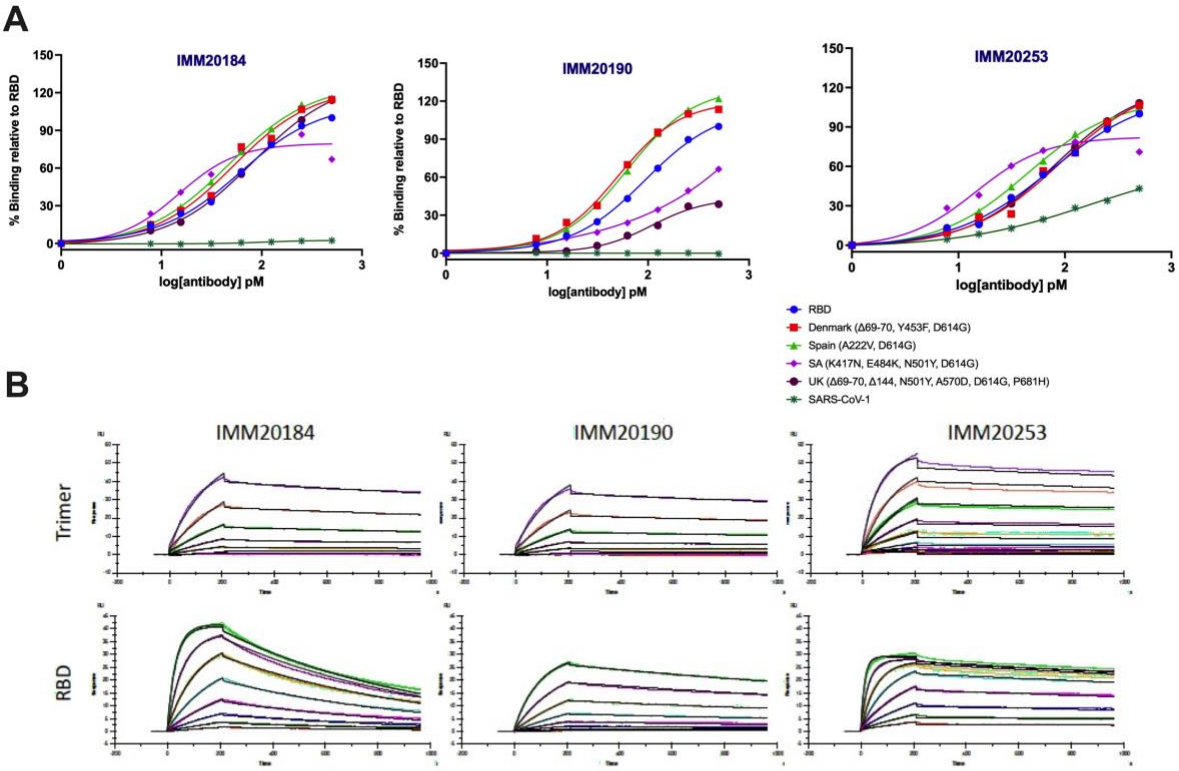

C

Ligand	Analyte	Kon (1/ms)	Koff (1/s)	KD (M)
IMM20184	Trimer	3.12E+04	2.29E-04	7.35E-09
	RBD	5.95E+05	1.31E-03	2.20E-09
IMM20190	Trimer	2.95E+04	1.95E-04	6.59E-09
	RBD	2.02E+05	3.76E-04	1.87E-09
IMM20253	Trimer	8.13E+04	1.17E-04	1.44E-09
	RBD	1.39E+06	2.18E-04	1.57E-10

Figure 4. Affinity of IMM20190, IMM20184 and IMM20253 antibodies. (A). Binding of IMM antibodies to soluble RBD proteins from SARS-CoV-1 and SARS-CoV-2 variants in a steady-state hTRF assay. (B). Antibody binding kinetics of IMM20184, IMM20190 and IMM20253 antibodies to soluble RBD and Trimer (REF variant) measured using Surface Plasmon Resonance (SPR). (C) KD, Kon and Koff values of IMM20184, IMM20190 and IMM20253 antibodies measured using a multi-cycle kinetics protocol assuming 1:1 interaction model.

A

Antibody	Main Bin
IMM20190	RBD, bin 1
IMM20184	RBD, bin 2
IMM20253	RBD, bin 3

B

Binding Reactivity (% WT)			
Mutation	IMM20190 Fab	IMM20184 Fab	IMM20253 Fab HS
K356A	82.2 (6)	61.5 (6)	7.1 (4)
Y365A	75.2 (3)	5.4 (3)	72.0 (3)
Y369A	107.0 (9)	13.2 (2)	14.0 (13)
N370A	63.4 (5)	7.5 (3)	72.4 (4)
A372S	127.3 (42)	3 (2)	99.9 (16)
F374A	64.8 (7)	7.4 (1)	70.8 (8)
K378A	87.9 (3)	6.7 (0)	66.9 (17)
V382A	61.9 (15)	15.6 (11)	49.3 (9)
S383A	110.8 (1)	0.4 (2)	86.3 (2)
P384A	111.5 (1)	2.1 (1)	112 (12)
K417A	5.6 (6)	96.2 (32)	113 (20)
D420A	4.6 (2)	65.5 (14)	69 (6)
L455A	4.5 (7)	170.6 (27)	114 (13)
F456A	2.3 (2)	79.7 (2)	64.8 (4)
N460A	9.4 (6)	76.3 (20)	89 (12)
R466A	70.8 (19)	78.7 (15)	5 (1)
Y473A	1 (7)	83.5 (26)	65.3 (7)
N487A	12.6 (6)	84.5 (7)	67 (31)
Y489A	3.1 (4)	73 (6)	65 (12)
N501A	12.9 (1)	93.4 (5)	80.1 (14)
Y505A	0.3 (4)	130 (9)	108.2 (11)

C

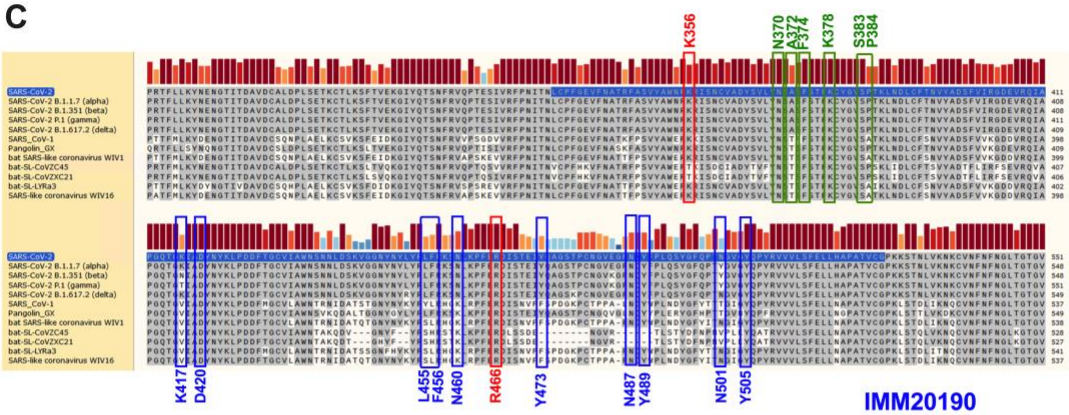

D

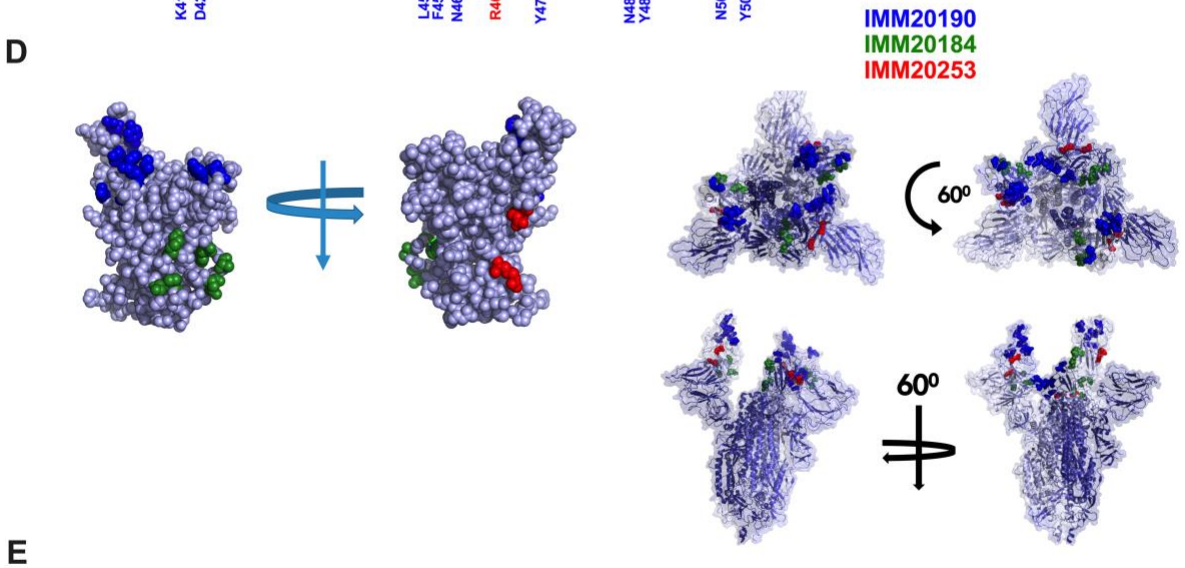

E

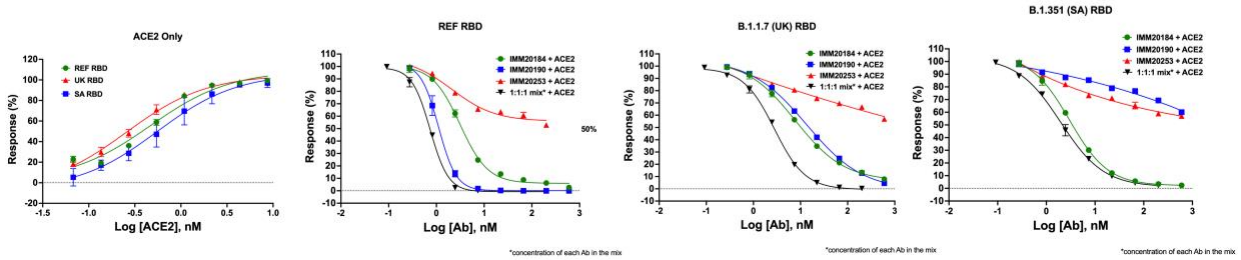

931

932 **Figure 5. IMM20190, IMM20184 and IMM20253 antibodies bind to rare non-competing**

conserved epitopes. (A) Bins of anti-Spike antibodies identified as non-competing binders to soluble RBD and Trimer proteins on Octet Qke. (B) Epitopes of IMM antibodies identified as binding pattern to a library of single-point RBD mutants expressed on the cell surface**.** Control Ab 1 and Control Ab2 are positive control antibodies. (C) Alignment of Spike protein sequences from CDC variants of concern with SARS-CoV-1 and closely related bat and pangolin coronaviruses. Epitopes of IMM20190, IMM20184 and IMM20253 are shown in blue, green and red. Highlighted sequence indicates the tested RBD protein. (D) Epitopes of IMM20190, IMM20184 and IMM20253 antibodies mapped on the RBD (left) and Trimer (right) structures (PDB: 7A97). Color scheme corresponds with panel (C). (E) 3-Ab cocktail inhibits RBD binding to its cellular receptor ACE2. ELISA-based receptor competition assay.

SUPPLEMENTARY MATERIALS

Supplemental Table 1. IC50 values for individual and combinations of IMM20184, IMM20190, and IMM20253 when measured by spot reduction assay using live virus

Antibody	BavPat	Alpha	Beta	Gamma
	IC_{50}	IC_{50}	IC_{50}	IC_{50}
IMM20184	40.5	25.4	83	16.6
IMM20190	0.6	2.25	>393	>393
IMM20253	40.2	0.35	165	12.1
IMM20184/IMM20190	0.4	1	Not Tested	
IMM20184/IMM20253	3.2	1.3		
IMM20190/IMM20253	0.5	0.6		
IMM20184/190/253 (IMM-BCP-01)	0.3	0.4	22	5.3

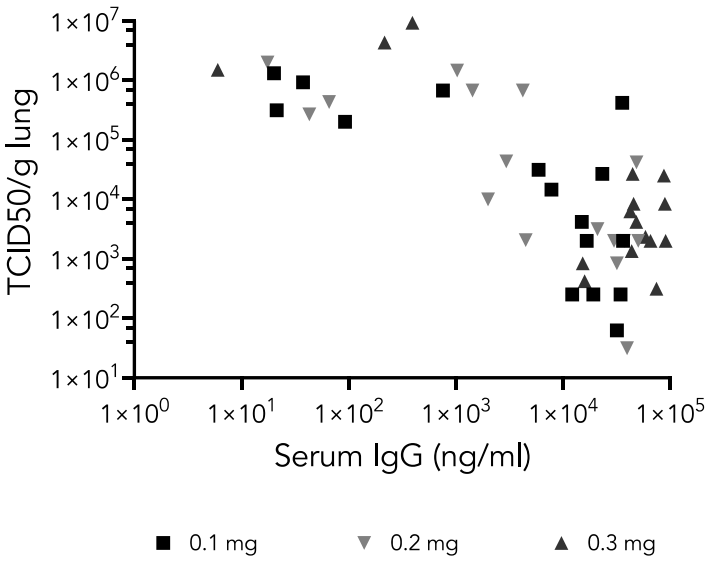

Supplemental Figure 1. Viral titer in lungs of infected hamsters depends upon Ab exposure. Syrian golden hamsters challenged with 3.3×10^5 TCID50 viral inoculation of a non-adapted WA_CDC-WA1/2020 SARS-CoV-2 isolate were treated with 3-Ab cocktail (IMM20184/IMM20190/IMM20253), at various dose levels, six hours post inoculation with virus. Lungs were harvested at day 4 post-treatment and viral titers were determined by TCID50 assay. Terminal levels of IgG in blood were quantified by anti-human ELISA.

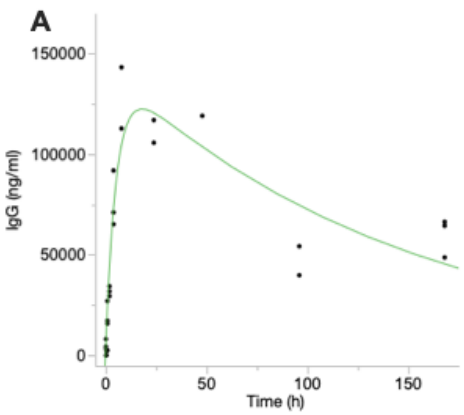

B

$$\left[\frac{[a * b * c]}{[c - b]}\right] * \left[\mathrm{Exp}\left[-b * \mathrm{Time\ (h)}\right] - \mathrm{Exp}\left[-c * \mathrm{Time\ (h)}\right]\right]$$

a = Area Under the Curve

b = Elimination Rate

c = Absorption Rate

C

Parameter	Estimate	Std Error	Lower 95%	Upper 95%
Area Under the Curve	20195524	3066443.2	14185405	26205642
Elimination Rate	0.0068647	0.0014516	0.0040197	0.0097098
Absorption Rate	0.18917	0.0368242	0.1169958	0.2613441

Supplemental Figure 2. Pharmacokinetics of the 3-Ab cocktail in hamsters. The 3-Ab cocktail (0.3 mg each) was administered i.p. into Syrian Golden hamsters and terminal bleeds (n = 4 per time point) were taken at 0.25, 0.5. 1, 2, 4, 8, 24, 48, 96, and 168 hours post administration. Total human IgG levels were determined by anti-human ELISA. (A) Pharmacokinetics in animals exhibiting < 1000 ng/mL IgG in serum at timepoints >30 minutes post-injection. Green line is the calculated curve using the formula shown in panel B. (C) PK parameters of data from panel A, calculated using formula shown in panel B.

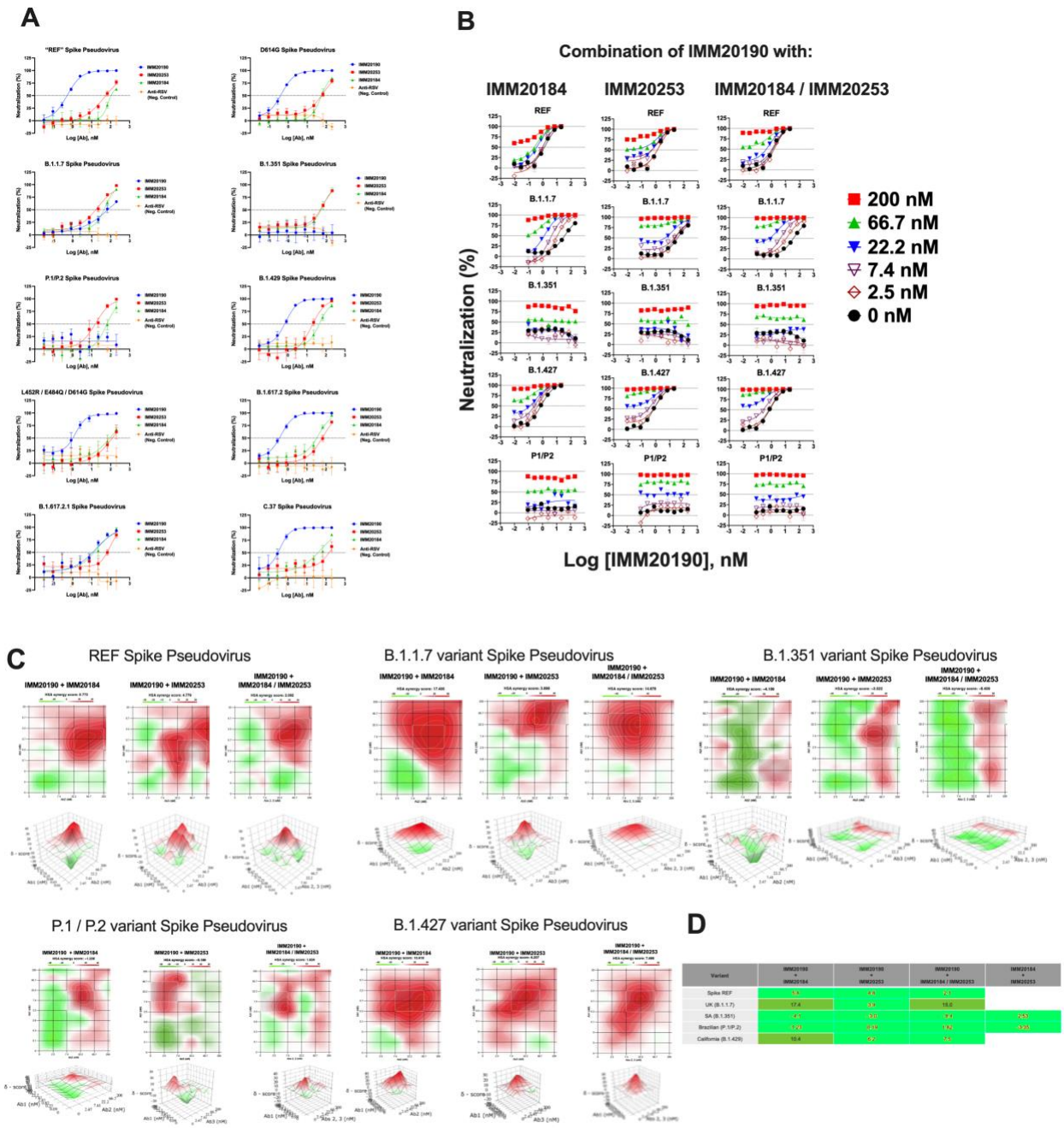

Supplemental Figure 3. Three selected antibodies have a synergistic neutralizing effect. (A) Neutralization properties of standalone IMM20190, IMM20184 and IMM20253 antibodies against 10 different Spike variant pseudoviruses. (B) REF, B.1.1.7 (alpha), B.1.351 (beta), P1 (gamma), and B.1.427 (epsilon) pseudovirus variant neutralization by IMM20190 combination

with either IMM20184, IMM20253 or both. (C) The Highest Single Agent (HSA) scores for 2-Ab and 3-Ab combinations. IMM20190 was mixed with IMM20184 and IMM20253 at 1:0.5:0.5 ratio. (D) HSA scores for two and three antibody cocktail.

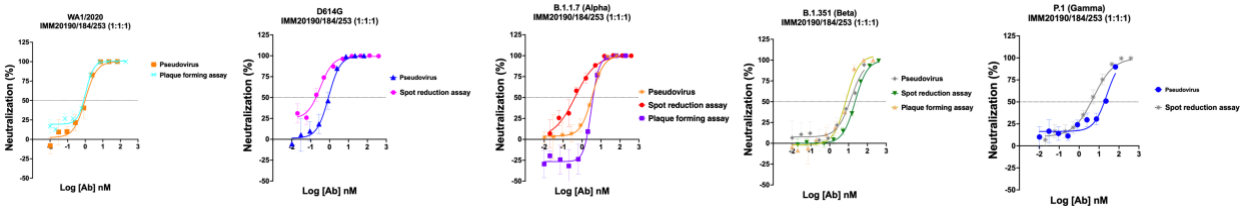

Supplemental Figure 4. **Neutralization of five virus variants by 3-Ab cocktail IMM-BCP-01 measured with different methods.** Pseudovirus, Spike pseudovirus neutralization assay. ViroSpot, an intact virus spot reduction assay. PFU (plaque forming units), a plaque formation assay using an intact virus.